Thin Films and Nanostructures of Niobium Pentoxide: Fundamental Properties, Synthesis Methods and Applications

Rozina Abdul Rani,[a*] Ahmad Sabirin Zoolfakar,[a,b] Anthony P. O'Mullane,[c] Michael W. Austin [a] and Kourosh Kalantar-zadeh[a*],

As one of the transition metal oxides, niobium pentoxide (Nb_2O_5) offers a broad variety of properties that make it a potentially useful and highly applicable material in many different areas. In comparison to many other transition metal oxides, Nb_2O_5 has received relatively little attention, which presents a significant opportunity for future investigations aimed at fundamentally understanding this material and finding new and interesting application for it. In this article, a general overview of Nb_2O_5 is presented which focuses on its fundamental properties, synthesis methods and recent applications, along with a discussion on future research directions relevant to this material.

1.0 Introduction

Niobium pentoxide (Nb_2O_5) is a metal oxide with great potential but to date this has yet to be fully realized. Interest in Nb_2O_5 can be dated back to the early 1940s when the polymorphs of Nb_2O_5 were first studied[1, 2]. Nb_2O_5 has many polymorphic forms which gives rise to an interesting series of structural phases. The phases are generally based on NbO_6 octahedral groups, forming various configurations from the rectangular blocks or columns [3]. Nb_2O_5 is relatively abundant in nature and has high corrosion resistance as well as being thermodynamically stable[4-6].

In the very early stages of research on Nb_2O_5, this material was mostly studied in bulk or thin layer forms as well as in suspensions[7-9]. The very first applications of Nb_2O_5, as a functional material, were investigated as catalysts, sensors and in electrochromism[10-17]. The unique performance of Nb_2O_5 in such studies was due to an understanding of its energy band diagram and the identification of crystal phases, which created the initial interest among researchers to explore more of this metal oxide's capabilities. Nb_2O_5 has grown in popularity in recent years and a variety of morphologies ranging from large size bulk crystals to different nanostructures have been reported[18-25]. In particular, nanostructured Nb_2O_5 offers high surface to volume ratios and quantum confinement effects that enable unique physical and chemical interactions to occur at the surface. As a result, such morphological manipulations significantly influence the optical and electronic properties of Nb_2O_5 leading to unique observations that are not seen in its bulk forms. Similarly, the chemical and physical properties of Nb_2O_5 can also be modified via other routes such as the incorporation of foreign ions, alteration of the crystal phase and post synthesis heat treatment[26-28] .

More recently, attention on Nb_2O_5 has gained more momentum due to applications other than electrochromism and catalysis. Especially, thin films and nanostructured Nb_2O_5 have been utilized in batteries, solar cells and other electronic devices such as memristors[20, 29-31]. However, most of these investigations are still in their infancy and much more research should be conducted to explore the true capabilities of Nb_2O_5 in these and other applications. Thus, more comprehensive studies on Nb_2O_5 should be conducted to provide further insight for researchers who intend to use this material for such applications.

In this review article, we present a broad review on Nb_2O_5 that includes its fundamental properties, synthesis methods and applications. Many of the common methods for synthesizing thin films and nanostructures of Nb_2O_5 are presented with a separate emphasis on liquid and vapour phase techniques. We summarize a selection of interesting applications that exploit Nb_2O_5 as the core material. In the final section, future outlooks on the possibilities to expand the areas of research and investigations using this material are elucidated.

2.0 Fundamental Properties

In the following section, an overview of the basic properties of Nb_2O_5 including crystal structure, electronic band diagram and electrical properties are presented. The fundamentals of the optical, mechanical and thermal properties of Nb_2O_5 are also discussed.

2.1 Crystal Structure

Nb_2O_5 is a transparent (due to its large band gap), air-stable and water-insoluble solid material with a relatively complicated structure that displays extensive polymorphism [32]. There are almost 15 polymorphic forms of Nb_2O_5 that have so far been reported, however, the most common crystal phases are generally pseudohexagonal (TT-Nb_2O_5), orthorhombic (T-Nb_2O_5), and monoclinic (H-Nb_2O_5) [3, 27, 32, 33]. As shown in Figure 1, after any relatively low temperature synthesis route amorphous Nb_2O_5 is normally obtained and then crystallizes at ~500 ºC into TT or T phases, at medium-temperature (~800 ºC) transforms into the M phase (tetragonal), and above ~1000 ºC it forms the H phase [34]. Despite this general temperature effect, the method of preparation, the nature of the starting material and the presence of impurities as well as interactions with other components also play decisive roles in the formation of the

resulting Nb_2O_5 crystal [3, 34]. H-Nb_2O_5 is the most thermodynamically stable crystal phase and is always produced when heated to temperatures above 1000 ºC, while the TT- and M- Nb_2O_5 forms are mostly metastable [3, 35]. It is important to mention that in some reports, Nb_2O_5 crystal phases have been re-designated as γ = T, β = M, and α = H [32]. However, there are still many inconsistencies regarding the identification of Nb_2O_5 crystal phases. Some investigators suggested that the M is simply disordered H phases [34] whereas M-Nb_2O_5 has been reported as a tetragonal Nb_2O_5 phase by Mertin *et al.* [35].

Some of the crystallographic properties of the different crystal phases of Nb_2O_5, with reference to their associated literature, are presented in Table 1. The unit cells of TT-, T- and H-Nb_2O_5 crystals are shown in Figure 2. A unit cell of TT-Nb_2O_5 contains half of the formula equivalent with a constitutional defect of an oxygen atom per unit cell (Figure 2a) [36]. Each niobium (Nb) atom is at the center of four, five or six oxygen atoms on the *ab*-plane and an Nb-O-Nb-O chain structure exists along the *c*-axis. As a result, the oxygen deficiency leads to the distortion of these polyhedra. Meanwhile, the T-Nb_2O_5 phase is constructed with the orthorhombic unit cell where each Nb atom is surrounded by six or seven oxygen atoms, creating distorted octahedra or pentagonal bipyramids (Figure 2b, 2d)[36, 37]. The polyhedra are connected by edge- or corner-sharing in the *ab*-plane and by corner-sharing along the *c*-axis [36]. The TT and T phases of Nb_2O_5 have quite similar X-ray diffraction patterns where the main difference is that some reflections that are split in T-Nb_2O_5 occur as one peak in the XRD patterns of the TT-Nb_2O_5 phase [32, 34]. The broadening of peaks in TT (or the splitting of the corresponding peaks in T) is due to the occupancy of niobium atoms in separate, but closely-spaced, equivalent sites in the T form, giving rise to the split peaks observed from certain reflections, and the ability of Nb to occupy either of these sites or places between the TT form, resulting in broadening of the same peaks in XRD patterns of TT [34]. These observations suggest that TT-Nb_2O_5 is a less crystalline form of T-Nb_2O_5, stabilized by impurities such as OH^-, Cl^-, or oxygen vacancies [34]. The monoclinic lattice of H-Nb_2O_5 contains ReO_3 type blocks of 3×4 and 3×5 groups containing NbO_6 octahedra (Figure 2c, 2e)[36, 38, 39]. These blocks are coupled by edge-sharing with a shift of half a unit cell dimension along the *c*-axis. NbO_6 units are connected by corner-sharing with each other within a block [36]. One of the 28 Nb atoms in each unit cell is present in a tetrahedral site, which occurs at some block junctions [32, 40]. M-Nb_2O_5 has similarity with the H-Nb_2O_5 crystal structure, which contains 4×4 of ReO_3 type blocks [3, 35]. This was concluded from the close relationship of the X-ray powder diagram of the M- and H- forms, which agree in a large number of reflections [3].

2.2 Band Energy Diagram and Electrical Properties

In electronic device development based on metal oxides, several properties of the incorporated materials are of utmost importance. These include the band energy diagram, electrical conductivity and dielectric permittivity. Nb_2O_5 is a wide band gap *n*-type semiconductor with a conduction band comprised of empty Nb^{5+} 4d orbitals and has a conduction band value that is 0.2 – 0.4 eV higher than titanium dioxide (TiO_2) [41]. Its band gap energy (E_g) values have been reported to be in the order of 3.1 (semiconducting) to 5.3 eV (insulating with conductivity of $\sigma = \sim 3\times10^{-6}$ S cm^{-1}) [42-44]. The ability to tune the band gap of Nb_2O_5 is possible and factors such as stoichiometry, crystallinity, heat treatment and incorporated foreign ions can dramatically influence the band gap energy. Previous studies have also shown that decreasing the dimensions of Nb_2O_5 into the nanoscale results in a blue shift of the energy gap, which can be attributed to the quantum-size effect [45]. Significantly, nanostructured Nb_2O_5 possesses grain dimensions that can critically influence the electronic structure of the material [46].

Viet *et al.* experimentally determined the band gap of crystalline Nb_2O_5 nanofibers (hexagonal, orthorhombic and monoclinic) which had been sintered at three different temperatures (500, 800 and 1100 ºC) [27]. Based on the Tauc plots derived from the absorption spectra in Figure 3a, they found that the hexagonal (labelled as H-Nb_2O_5), orthorhombic (labelled as O-Nb_2O_5) and monoclinic (labelled as M-Nb_2O_5) forms of Nb_2O_5 exhibited band gaps of 3.85, 3.77 and 3.79 eV, respectively [27]. Meanwhile, Abe reported that the powder-synthesized orthorhombic Nb_2O_5 had a band gap value of 3.4 eV, while that of monoclinic Nb_2O_5 gave a reported value of 3.1 eV[26]. Moreover, the same author also investigated the effect of doping on the energy band gap of Nb_2O_5 by incorporating different concentrations of germanium (Ge) in the monoclinic Nb_2O_5 films. The optical absorption edge of the monoclinic Nb_2O_5 which is derived using the Kubelka-Munk function was observed at 3.1 eV without Ge doping which shifted up to 3.35 eV as the Ge concentration was increased [26]. The incorporation of tungsten and molybdenum into Nb_2O_5 has also been reported as well as the treatment of Nb_2O_5 with hydrogen peroxide in order to manipulate the band gap of Nb_2O_5 [47].

Recently, Liu *et al.* fabricated single-crystalline nanoporous Nb_2O_5 nanotubes using a two-step solution route; the growth of uniform single-crystalline Nb_2O_5 nanorods and the following ion-assisted selective dissolution along the [001] direction [48]. The band gap of Nb_2O_5 nanotubes and nanorods are 3.97 and 3.72 eV, respectively (Figure 3b). As mentioned previously, the 0.25 eV difference was due to the blue shift of the absorption edge for the porous nanotubes compared to solid nanorods which is due to the quantum size effect in hollow Nb_2O_5 nanotubes [48]. The same effect was also observed by Brayner *et al.* in the transmission spectrum of Nb_2O_5 particles: a significant blue shift of the absorption edge was observed and therefore the band gap increased from 3.4 eV to 4.2 eV, as the particle size of Nb_2O_5 decreased from about 40.0 nm to 4.5 nm [49]. The effect of grain size on the band gap of Nb_2O_5 was also presented by Agarwal *et al.* [50], although they suggested that the energy of the absorption edge is influenced by both the size and local coordination of the grains.

Table 1: Lattice parameters of TT, T, M and H phases of Nb_2O_5.

Crystal phase	Space group	Lattice constant			Temperature (ºC)	Refs.
		a (Å)	*b* (Å)	*c* (Å)		
Pseudohexagonal	P6/mmm	3.60	3.61	3.92	500	[27] [51] [52]
Orthorhombic	Pbam	6.19	3.625	3.94	-	[51] [53, 54]
Tetragonal	*I*4/mmm	20.44	3.83	3.82	900	[35] [55]
Monoclinic β = 119.9° ± 0.4°	P12/m1, P2, P2/m	21.14	3.82	19.45	>1000	[27] [3, 56] [1] [53] [57] [58]

In Nb_2O_5, like other semiconductors, the concentration of charge carriers is directly related to the defect structure of the metal oxide which is dependent on temperature and oxygen pressure [59]. Greener *et al.* conducted a detailed analysis of the relation between conductivity of α-Nb_2O_5 (monoclinic) and temperature under ambient oxygen pressure [60]. As presented in Figure 4, they showed that an increase in temperature and decrease in oxygen partial pressure increased the conductivity of α-Nb_2O_5. These results are in excellent agreement with the measurements by Kofstad and Chen *et al.* [61, 62].

To scale down the physical dimensions of integrated circuits, investigating of high-κ (high permittivity) materials is important for reducing the leakage current in integrated capacitors and gate insulators. Based on experimental measurements and first-principles calculations, Clima *et al.* reported that the relative dielectric permittivity of sol-gel deposited Nb_2O_5 to be 77 for the orthorhombic phase, 58 for the δ_A-hexagonal phase and 38 for the δ_B-hexagonal phase [63]. They found that the dielectric constant of Nb_2O_5 strongly depended on the crystal structure and the inspection of the permittivity tensors revealed that the dielectric constants are anisotropic. More recently, Nb_2O_5 thin films were grown by atomic layer deposition using novel precursor chemistry for metal-insulator-metal (MIM) capacitors with a relative permittivity of 28 [64]. However, after annealing at 650 ºC, the films' relative permittivity values increased to 45–50 due to the enhanced crystallinity of the films. In addition, Cavigliasso *et al.* reported that the dielectric constant of Nb_2O_5 films created electrochemically by electrooxidation depended on the electrolyte used, and resulted in dielectric constant values over the range of 49 to 120 [65].

Electronic mobility is another important parameter in semiconductor device development especially for field effect transistors (FETs). A mobility value of 7×10^{-2} cm^2/Vs for α-Nb_2O_5 at a temperature of 1200 ºC was reported by Yahia [66]. Further, it has been shown that the mobility is increased by increasing the temperature.

2.3 Optical Properties

As mentioned in section 2.2 the band gap of Nb_2O_5 ranges between 3.1 and 5.3 eV. As a result, Nb_2O_5, depending on its crystallinity and grain morphology can efficiently absorb light in the near UV and UV regions of the spectrum or it can be used as a transparent material to UV light. Nb_2O_5 has been identified as being capable of reversible and rapid coloration in the presence of intercalating ions such H^+ and Li^+ ions. It has been reported that this phenomenon can modulate the Nb_2O_5 optical transmission from a quasi-transparent state (T~ 85 %) to less than T~ 10 % in the ultraviolet (UV), visible or near infrared (IR) range, and can exhibit either a blue or brown colour depending on the crystallinity of the film [17, 67-69].

The optical properties of Nb_2O_5 have been experimentally studied *via* various techniques such as spectrophotometry and spectroscopic ellipsometry [70-73]. The refractive index value of Nb_2O_5 films has been reported to be in the order of 2 to 2.3 [71, 73]. Also the crystallinity of the film plays a significant contribution to the refractive index of the material as it decreases from 2.30 to 2.20 after being annealed from room temperature to 700 ºC [70].

2.4 Mechanical Properties

Besides electronic and optical properties, an investigation of the mechanical properties of Nb_2O_5 is also of major importance for the fabrication of electronic devices especially for the development of flexible mechanical devices and actuators such as micro electro-mechanical system (MEMS) devices. Stress or strain commonly occurs in thin films depending on the deposition process and constraints imposed by the substrate. The average hardness (H) and Young's modulus (E_r) values of as-sputtered Nb_2O_5 films have been reported to be in the order of 5.6 to 6.8 GPa and 117 to 268 GPa respectively, which is again influenced by the crystal phase [70, 74].

In flexible device applications, the bending test is essential to perform in order to monitor the effects of stretching on the device output and to make sure that all the component layers are stable even after several thousand flexes. Some of the appropriate flexibility tests and other related mechanical tests for electronic devices have been described in detail elsewhere[75-78]. Hota *et al.* have demonstrated that sputtered Nb_2O_5 thin films (~50 nm thickness) on flexible polyethylene terephthalate (PET) substrates show high mechanical flexibility in a repetitive bending test [79]. A collapsing radius test, which is one of the common bending test techniques, was applied to MIM capacitors based on sputtered Nb_2O_5 thin films, and the obtained results show endurance of up to 2500 flexes.

2.5 Thermal Properties

In an electronic system, heat dissipation is an acute problem due to miniaturization and the increasing power of microelectronic circuits. Thus, thermal conductor materials with high thermal conductivity and a low coefficient of thermal expansion (CTE) are essential for the purpose of heating and cooling. For Nb_2O_5, a limited number of studies have been carried out on its thermal properties. An investigation of the high-temperature thermal expansion of monoclinic Nb_2O_5 was conducted using X-ray and dilatometric techniques by Manning *et al.* [80]. The results revealed that the lattice thermal expansion of Nb_2O_5 is anisotropic where the mean coefficients in the *a*, *b*, and *c* directions were 5.3×10^{-6}, 0 and 5.9×10^{-6} $ºC^{-1}$, respectively. Previous works also demonstrated the low thermal expansion behaviour of Nb_2O_5 over the temperature range of 20 to 1000 °C [81, 82]. In addition, another report demonstrated a

negative thermal expansion of Nb_2O_5 at relatively high temperatures as large as 500 °C [83, 84] which was attributed to the recombination of the microcrack network formed during cooling. There are just a few reports regarding the Seebeck coefficient of Nb_2O_5 [85]. It has been reported that its Seebeck coefficient changes from −0.5 to −1.2 mV/°C when the temperature changes from 500 to 1000 °C.

3.0 Synthesis of Nb_2O_5

Nb_2O_5 has been synthesized using many approaches and the key motivation in choosing the right synthesis method is its capability in tuning the properties of Nb_2O_5 (mostly crystal phase and morphology). In this section, we have chosen the most common synthesis methods and classified them into two major categories: liquid and vapour phase based. In addition, complementary methods are also presented.

3.1 Liquid Phase Deposition Methods

Liquid phase techniques include methods such as hydrothermal, anodization, sol-gel and electrodeposition. These methods are chosen due to their low capital cost, relatively low operating temperatures and high control over Nb_2O_5's properties in comparison to vapour phase deposition techniques, which is crucial for the fabrication of cheap and low-heat-tolerant substrates.

3.1.1 Hydrothermal and Solvothermal Methods

Hydrothermal (in water) and solvothermal (in other solvents such as acetone and isopropyl alcohol) synthesis techniques are simple methods that have been utilized to produce metal oxide crystals. These methods involve an ionic source of metal in a solution which is heated at an elevated temperature for a certain period of time. For the deposition of Nb_2O_5, the solution of Nb^{5+} ions is sourced either *via* the interaction of niobium metal in an acid or base or the dissolution of a niobium salt such as niobium chloride, niobium ethoxide, or ammonium niobium oxalate (see Table 2). The solvents are then heated at a temperature in the range of 100 – 600 ºC for duration of a few hours to several days (see Table 2). Normally, this process allows the nucleation and growth of naturally crystalline Nb_2O_5 to proceed. Nanostructured Nb_2O_5 such as nanorods, nanobelts, nanospheres and other configurations are also possible to be synthesized using these hydrothermal or solvothermal methods. A brief summary of the type of nanostructured Nb_2O_5 that can result from such methods is presented in Table 2. Figure 5 presents a selection of the type of Nb_2O_5 nanostructures that have been achieved using a few selected hydrothermal or solvothermal methods. Due to the high-aspect-ratio properties and high surface area that can be obtained, these methods offer great potential for obtaining Nb_2O_5 that can be used in various specific applications including lithium-ion batteries, dye-sensitized solar cells and photocatalysis applications which will be explained in the later sections [38, 86-89].

3.1.2 Anodization Method

Anodization is one of the most widespread nano-fabrication methods due to its capability of forming highly porous and ordered oxide morphologies[90, 91]. In a typical anodization experiment, a potential is applied between two electrodes; a working and counter electrode, which are both immersed in a liquid electrolyte. An electrical current or voltage is then applied, which results in electrochemical reactions occurring on the surface of the metal electrode (working electrode) and an oxide film is formed. The growth and morphology of the anodic oxide film strongly depends on the applied anodization potential, the composition of the electrolyte (aqueous, organic solvent with or without water and etching agent content), the electrolyte temperature, and the anodization duration. The as-anodized Nb_2O_5 films are mainly amorphous and require a post-annealing treatment to be converted into highly crystalline and stoichiometric Nb_2O_5.

Studies on anodic Nb_2O_5 films have been conducted as early as the 1960s. Draper *et al.* presented work that was undertaken to study the anomalies in published work on the structure of the anodic films formed on niobium (Nb) and how the physical nature of the film material might influence the growth rate [92]. Later, a study on anodic Nb_2O_5 film properties (i.e., resistivity, dielectric constant) was presented by Wood *et al.* [93]. Other early studies on anodized Nb_2O_5 surface morphology and crystallization analysis using an electron microscope, electron-beam crystallization and reflection electron diffraction have been reported elsewhere [94, 95].

The anodization of Nb has been intensively studied in various electrolytes (sulfuric acid, phosphoric acid, NaOH, Na_2CO_3, HF, glycerol, ethylene glycol, fluoride, and phosphorus based solutions). Most of the reported anodic Nb_2O_5 films consist of highly nanoporous structures on a Nb foil substrate[96-103]. In one of the most important reports, conducted by Habazaki *et al*, the effect of water content on the formation of porous Nb_2O_5 anodized in a K_2HPO_4-glycerol electrolyte as well as at elevated temperature was discussed [96]. They showed that by reducing the water content to 0.08 mass%, the porous film growth rate markedly increased (as thick as 28 μm) at 160 °C, which is associated with the increased field strength by a higher concentration of phosphorus species. Ou *et al.* later reported the creation of a three dimensional (3D) vein-like nanostructured network in an electrolyte consisting of ethylene glycol with NH_4F and small content of water (~4%) (Figure 6a) [23]. In all of these processes, an elevated temperature was applied based on the hypothesis that it increases the ion diffusion rate during the anodization process.

Apart from a nanoporous structure, microcones were also obtained by Nb anodization in an electrolyte containing deionized water with a low concentration of HF or in a glycerol electrolyte containing K_2HPO_4[104-107]. Wei *et al.* reported anodized nanotubes of Nb_2O_5 up to 4 μm thick by optimizing the anodization of Nb in an NH_4F based glycerol electrolyte [108]. Recently, Lee *et al.* reported the first anodization procedure to produce highly ordered nanochannels of Nb_2O_5 grown in glycerol containing K_2HPO_4 electrolyte also at 180 ºC [109]. They showed that the channel length could be adjusted from a few hundred nm to several tens of μm. Lee *et al.* were successful in growing films of thick nanochannels of Nb_2O_5 by pre-heating the electrolyte at 200 ºC before conducting the anodization in order to reduce the water content [109]. Other reports on anodic nanochannelled Nb_2O_5 films were also reported by Abdul Rani *et al*. (Figure 6b) [22]. Moreover, reports on nanoporous Nb_2O_5 films and nanochannelled Nb_2O_5 films obtained from anodizing Nb films, which were RF sputtered on fluorine doped tin oxide (FTO) glass substrates, have also been demonstrated recently (Figures 6c and d) [69, 110, 111].

3.1.3 Sol-gel Methods

The sol-gel process is a simple wet-chemical method that involves the conversion of selected monomers into a colloidal solution (sol). The sol acts as the precursor for the formation of an integrated network (or gel) which can be eventually used for creating discrete particles or connected networks [112]. The deposition of the final oxide films using a sol-gel process is normally conducted by methods such as dip- or spin coating, electrospinning, or drop-casting. Despite its simplicity, there are some limitations as well. The bonding can be weak, resulting in inhomogeneity in subsequent films. There are also certain difficulties in controlling the reaction rate and porosity[113-115].

The preparation of Nb_2O_5 *via* sol-gel methods was first reported by Alquier *et al.* in 1986 [112, 116]. The typical precursors used for Nb_2O_5 films synthesised via sol-gel processes are quite similar to the hydrothermal or solvothermal methods, containing a mixture of niobium salt and its solvent. The sol-gel Nb_2O_5 films generally require a post-annealing treatment in order to induce crystallinity. Schmitt *et al.* have reported a sol-gel based Nb_2O_5 thin film by dissolving $NbCl_5$ powder in butanol and acetic acid [68]. The Nb_2O_5 films were deposited by dip-coating and then annealed at 400 – 600 ºC to obtain the TT crystal. Similar procedures have also been demonstrated by other researchers using different precursors such as niobium ethoxide and ammonium niobium oxalate[4, 29, 67, 117-125]. As can be seen from Figure 7a, b and c, films consisting of nanoparticle structures are normally obtained by dip or spin coating deposition techniques[121, 124]. Different structural morphologies of Nb_2O_5 have been demonstrated by Viet *et al.* using electrospinning which resulted in Nb_2O_5 nanofibers as shown in Figure 7d, e and f [27]. These nanofibers were synthesized from a polymeric solution prepared from polyvinylpyrrolidone (PVP) and niobium ethoxide in ethanol and hydrolyzed using acetic acid.

3.1.4 Electrodeposition

Electrodeposition can be considered as a common method for the fabrication of nanostructured materials in the form of thin films, powders and composites [126]. This process often involves a two electrode configuration immersed in an electrolyte, where a metal oxide film forms at the cathode in contrast to the anodization method described in section 3.1.2. The aqueous electrolyte used for Nb_2O_5 electrodeposition generally contains niobium ions and hydrogen peroxide (H_2O_2) [127, 128].

In one of the very first electrodeposition reports, Zhitomirsky performed electrodeposition by applying a constant current density of 20 mA/cm^2 at 1 ºC for 20 min in an electrolyte mixture of $NbCl_5$ and H_2O_2 [126, 127]. The produced Nb_2O_5 thin films exhibited microporosity with a thickness of 0.3 μm, were crack free and adhered well to the substrate**.** Non-aqueous electrolytes can also be used in electrodeposition but they need to have some supporting electrolyte to allow the conduction of current. Kamada *et al.* added 0.01 M iodine (I_2) and bromine (Br_2) into acetone as an electrodeposition electrolyte to obtain Nb_2O_5 films [25]. Although the addition of I_2 into acetone induced anodic oxidation of the metal anode, subsequent electrochemical dissolution and cathodic deposition did not take place. The addition of Br_2 has been found to promote both anodic dissolution and electrodeposition of Nb species.

3.2 Vapour Phase Deposition

In general, vapour phase deposition is a process to fabricate layers of materials from the condensation of their vaporized sources under favourable environments. There are two major categories of vapour phase deposition: physical vapour deposition (PVD) and chemical vapour deposition (CVD).

3.2.1 Physical Vapour Deposition (PVD)

PVD techniques are used for depositing a wide variety of films with thicknesses which vary from a few angstroms to several millimetres. The deposition of a film is through the evaporation of the precursors into a vapour phase by physical approaches such as ion bombardment, heat, electron beam or laser irradiation followed by the condensation of the vapour phase onto the required substrate [129, 130].

So far, sputtering has been the most reported PVD technique to deposit Nb_2O_5 films. Generally, Nb_2O_5 films can be obtained using direct current (DC) [72, 131-136] or radio frequency (RF) [18, 132, 137-143] sputtering techniques with metallic niobium (Nb) [72, 131, 133-135, 138-142, 144-146] or Nb_2O_5 [18, 137, 143] targets in the presence of carrier gases such as argon (Ar) in oxygen (O_2) environments. These techniques are capable of producing Nb_2O_5 films or nanostructured forms with preferred dimensions, crystallinity, nanoscale grain sizes and morphologies by controlling the deposition parameters (i.e; pressure, distance between the target and the substrate, substrate temperature, discharge voltage, RF power) during the sputtering process [147]. Post-annealing treatment in a controlled gas environment is usually used to enhance the crystallinity of the sputtered films. Even though sputtering can produce high-quality films, this technique is time consuming due to its low deposition rates (typically in the μm/hour range) [148].

In addition to sputtering, other PVD techniques have been established to fabricate Nb_2O_5 films such as ion-beam assisted deposition [70, 71, 149, 150], thermal evaporation [151], pulsed magnetron sputtering [145, 152] and pulsed laser deposition (PLD) [20, 153-155]. Pulsed magnetron sputtering and PLD have been found to increase the deposition rate of Nb_2O_5 films to the order of tens of microns per hour and are also able to conserve the original stoichiometry of a bulk target to the deposited film [148, 153]. It is also possible to obtain high aspect ratio nanostructures such as nanobundles that have been shown by Ghosh *et al.* using PLD process (Figure 8) [20].

3.2.2 Chemical Vapour Deposition (CVD)

CVD techniques are also commonly used in the formation of films (in particular conformal coatings) and nanostructures[156, 157]. Nb_2O_5 thin films (nanostructured and compact) have been successfully synthesized using CVD techniques such as metal-organic CVD (MOCVD) [158, 159], plasma-enhanced CVD (PECVD) [160], atmospheric pressure CVD (APCVD) [161, 162], and vapour-liquid-solid (VLS) growth mechanisms under vacuum or atmospheric conditions [163].

Table 2: Summary of Nb_2O_5 nanostructures obtained using hydrothermal and solvothermal processes and their synthesis conditions.

Morphology	Dimension (nm)	Solution	Temperature (ºC)	Duration (h)	Crystal phase
Nanograins, nanorods and nanoplatelets [164]	D: 50 - 80 L:> 1000	$NbCl_5$ and ethanol in cyclohexanol	200 - 240	8 - 90	Orthorhombic for T > 225 ºC
Nanoparticles [165]	D: 18 - 35	$NbCl_5$ in anhydrous benzyl alcohol	250	72	Pseudohexagonal
Nanopowder [166]	L: < 80	Niobium pentabutoxide in toluene	300	2	Pseudohexagonal
Nanobelts [167]	T: ~15 W: ~60	Nb powder in urea	170 - 200	24 -336	N/A
Nanocables and nanorods [168]	D: 50 - 80 L:> 1000	$NbCl_5$ and ethanol in cyclohexanol	200 - 240	8 - 90	Orthorhombic
Nanorods [169]	D: 50	Nb powder in distilled water	200	72 - 720	Orthorhombic
Nanosheets [86]	T: 3 -5	NbO_2 powder in distilled water and ethanol containing 1 M urea	130	72 - 720	Orthorhombic and monoclinic
Mesoporous [170]	-	$NbCl_5$ in ethanol mixed with triblock copolymer dissolved in distilled water	110	24	Orthorhombic after calcined at 600 ºC
Mesoporous spheres [171]	D: 400 - 500	Niobium ethoxide, diethylene glycol and acetone in water	180	4 - 12	Pseudohexagonal
Nanospheres [89]	D: 20 – 50	Ammonium niobate oxalate hydrate in distilled water	580	1	Pseudohexagonal
Nanorods [89]	D: 5 – 20 L: 100 - 500	Ammonium niobate oxylate hydrate and oleic acid in trioctylamine	180	2 - 6	Pseudohexagonal
Nanotrees [172]	D: 30 - 500	Lithium hydroxide in HF acid	150 - 200	20 - 40	Pseudohexagonal
Nanorods [173]	D: 50 - 100	Ammonium fluoride	150	24 - 144	Orthorhombic for duration > 48 h
Nanoparticle [88]	D: 9 - 35	Ammonium niobium oxalate and hydrogen peroxide in distilled water	100 - 175	2 - 24	Orthorhombic
Hollow microspheres [174]	D: 1000 - 2000	Nb_2O_5, LiOH and $NH_3 \cdot H_2O$ in H_2O_2	240	24	Pseudohexagonal after calcined at 500 ºC
Nanocomposite [87]	D: 25 - 29	Ammonium niobate oxalate hydrate, sucrose and HCl in deionized water	180	12	Pseudohexagonal
Nanorods [38]	D: 22 L: 230	$NbCl_5$ in HCl	210	24	Monoclinic after calcined at 450 ºC

Generally, to deposit the Nb_2O_5 films, precursors such as $NbCl_5$ and pentaethoxy niobium $[Nb(OC_2H_5)_5]$ are transported using reactant/carrier gas species into the reaction chamber, and subsequently decomposed on the surface of a heated substrate[160].

O'Neill *et al.* showed that the Nb_2O_5 film growth strongly depended on the substrate temperature when deposited by the CVD reaction of $NbCl_5$ with ethyl acetate [161]. At lower temperatures (400–500 ºC), the resultant films tended to be uniform, forming layered growths. Deposition at temperatures higher than 500 ºC produced hazy films with fairly uniform columnar nanostructure associated with Volmer-Webber growth throughout the films. At 600 ºC a milky appearance was observed, which was attributed to the films being comprised of uniform inter-grown rods that were virtually all aligned

perpendicular to the substrate surface. These results indicated that the changes in the morphology of the films with substrate temperature were related to the number of nucleation sites available and the delivery rate of the precursor [161]. In another approach, the initial niobium pentaisopropoxide $[Nb(O^iPr)_5]_2$ precursor was decomposed at 950 ºC onto polycrystalline alumina substrates, which resulted in one-dimensional monoclinic Nb_2O_5 nanorods [163]. Other studies using CVD methods offer excellent alternatives to produce layered Nb_2O_5 especially for fibre coating applications[158, 162].

Furthermore, spray pyrolysis which is a typical aerosol-assisted CVD is among one of the most well utilized methods to synthesis thin or thick Nb_2O_5 films[19, 175-178]. This method has the capability of forming large-scale thin films by using a simple apparatus with large productivity. With regard to the substrate temperature, a post annealing treatment is usually required to obtain highly crystalline Nb_2O_5 films if a low temperature is applied during the deposition.

3.3 Thermal Oxidation

Thermal oxidation is a simple fabrication technique. The starting material to fabricate Nb_2O_5 is normally Nb metal/foil or powder, and then the thermal oxidation is performed by heating the sample in a furnace at a temperature as high as 1000 ºC generally in a O_2 or oxidizing rich environment [16, 21, 55, 179-183]. The technique forces the oxidizing reagent to diffuse into the substrate at a high temperature and react with it. The nanostructured Nb_2O_5 is directly grown onto the surface of a Nb substrate. The resultant structures can vary from compact films to nanowires and core-shell structures. It has been reported that nanowires as long as 20 μm can be produced by this approach[180, 182]. The growth of these nanostructures can be controlled by optimizing the temperature, time, metal-catalyst and gas atmosphere during the synthesis process [184].

4.0 Applications

Applications of Nb_2O_5 normally involve the utilization of some unique properties of Nb_2O_5 such as its electronic and optical properties or biocompatibility which may be enhanced by the modification of Nb_2O_5 films such that they significantly enhance the performance of a device. In the following sections, some of the most common applications of Nb_2O_5 that have been reported in the literature are presented.

4.1 Solar Cells and Light Emitting Diodes

Nb_2O_5 films are promising candidates for developing different types of optical devices, including solar cells based on dye-sensitized and heterojunction architectures as well as light emitting diodes (LEDs).

Since their discovery by Grätzel in 1991, dye sensitized solar cells (DSSCs) have been extensively studied as they offer the potential for clean, reliable, cost effective and on-site energy generation [185]. Increasing the efficiency of DSSCs depends on improving every single element in their structure, including: photoanode, dye, electrolyte and counter-electrode. However, the development of the most suitable photoanode will still have the most significant impact on the DSSCs's performance [185]. Nb_2O_5 has recently drawn considerable attention as a promising photoanode in view of its wider band gap (due to its higher conduction band edge) as well as comparable electron injection efficiency and better chemical stability in comparison to titanium oxide (TiO_2) [23, 41, 186]. These properties of Nb_2O_5 can potentially enhance the DSSCs' efficiency by increasing the open circuit voltage (V_{oc}) and photoconversion efficiency (η) [187].

Several studies have been reported on the synthesis of Nb_2O_5 photoanodes which were obtained using hydrothermal, chemical anodization, sol-gel coating and PLD techniques [17, 20, 22, 23, 38, 110, 167, 188-190]. The details are summarized in Table 3. To date, the highest conversion efficiencies of more than 6% have been exhibited by devices with a hydrothermally grown Nb_2O_5 photoanode with the optimum thickness of ~11 μm [38]. Ou *et al*. and Rani *et al.* have established an anodization method to obtain Nb_2O_5 nanovein-network photoanodes with large surface areas and low number of impurity defects for DSSCs [23, 110]. The photoanodes with no detectable impurities exhibited longer electron lifetimes, indicating more suitability in preventing charge recombination and possible enhancement of the conversion efficiency (Figure 9). However, the efficiency of the overall devices incorporating these photoanodes was still relatively low (~ 3.5 to 4.1 %) which was attributed to the lack of the optimisation of the thickness of the Nb_2O_5 frameworks.

Additionally, several researchers have applied Nb_2O_5 films as a blocking layer in DSSCs. Thin Nb_2O_5 films fabricated by spray pyrolysis, sputtering, sol-gel and dip coating methods have been used as potential blocking layers between the contact electrode and the TiO_2 layer, improving the V_{oc} which created a better conversion efficiency for TiO_2 based DSSCs [176, 191-194]. Furthermore, it has been shown that a Nb_2O_5 film could play an essential role in increasing the efficiency of the DSSCs as a layer between the TiO_2 photoanode and electrolyte[195-197]. This increase was attributed to the coating which either prevented the recombination of electrons and holes due to the barrier effect or the change in the energy level of the TiO_2 conduction band [197]. However, other investigations have disregarded those factors and claimed that the improvement in the performance of the cell could be attributed to an enhancement in the charge injection efficiency promoted by Nb_2O_5 [195]. Nb_2O_5 has also been incorporated as a counter electrode in DSSCs. Wu *et al.* and Lin *et al.* have reported a significant conversion efficiency between 4.65 to 5.82 % in DSSCs using a Nb_2O_5 counter electrode with a TiO_2 photoanode [198, 199]. In these studies, the types of gases used during the annealing treatment and changes in crystallinity of the Nb_2O_5 counter electrode were reported as a factor that influenced the DSSCs' efficiency.

For polymer based bulk heterojunction solar cells, Nb_2O_5 thin films commonly act as electron transport layers[200, 201]. It has been found that Nb_2O_5 films are compatible with and have good adhesion properties to many polymer layers [200].

Table 3: Summary of DSSCs based on Nb_2O_5 nanostructured films featuring their typical performance data.

Photoanode	Efficiency (%)	*Voc* (V)	*Jsc* (mA/cm^2)	Thickness / substrate	Refs.
Nb_2O_5 with nanochannel structures (anodization process – Nb foil as a substrate)	4.48	0.639	17.6	10.0 μm / Nb foil	22
Nb_2O_5 with nano-vein networks	3.45	0.635	8.72	5.0 μm / FTO glass	110
Nb_2O_5 with nanochannel structures (anodization process – RF sputtered Nb metal on FTO as a substrate)	2.20	0.670	6.91		
Nb_2O_5 with micro-mountain and nano-forest pancake structures (anodization process)	3.35	0.59	10.66	27.7 μm / Nb disk	190
Nb_2O_5 nanorod film (By transforming $Nb_3O_7(OH)$ hydrothermal into Nb_2O_5 nanorods after annealing)	6.03	0.749	12.20	11.2 μm / FTO glass	38
Nb_2O_5 nanoparticle	4.68	0.662	11.57	12.1 μm / FTO glass	
Nb_2O_5 with nano-vein networks (anodization process – Nb foil as substrate)	4.1	0.701	10.00	4.0 μm / Nb foil	23
Nb_2O_5 nanoforest by PLD	2.41	0.710	6.65	5.9 μm / FTO glass	20
Nb_2O_5 thin film deposited by spray pyrolysis	0.98	0.455	1.6	ITO glass	19
Nb_2O_5 nanobelts (powder-air thermal)	1.42	0.580	3.93	10.0 μm / FTO glass	167
Nb_2O_5 sol-gel film with polymeric ligand and carbon soot deposited by spin coating	4.00	0.665	12.20	15.5 μm / FTO glass	17
Nb_2O_5 colloids and adding hydroxypropyl cellulose (Hydrolysis and spin coating – autoclave technique)	4.00	0.595	9.70	15.5 μm / FTO glass	202
Nb_2O_5 sol-gel film deposited by spin coating	2.20	0.610	7.00	6.0 μm / FTO glass	121
Nb_2O_5 nanoporous film (powder-air thermal)	2.00	0.630	4.90	8.0 μm / FTO glass	188
Nb_2O_5 ordered needles film (Colloidal suspensions were made from hydrolyzed niobate solutions by an autoclave method)	-	0.400	0.53	6.0 μm / ITO glass	189

Wiranwetchayan *et al.* reported that very thin Nb_2O_5 films between the electron collecting electrodes and active layers were necessary to promote the formation of continuous uniform active layers and thus blocking the holes in those layers from being recombined with the electrons in the collecting electrode [201]. However, further investigations of such polymeric solar cells should be considered in order to obtain higher conversion efficiencies.

The capability of Nb_2O_5 films have also been studied in LED applications[203, 204]. Su *et al.* applied Nb_2O_5 and SiO_2 films as high and low refractive indices of omnidirectional high reflector (ODR) in white LEDs, respectively [204]. The Nb_2O_5 and SiO_2 pair was chosen due to their high transparencies in the visible and UV wavelength ranges[71, 204]. They observed that the leaked UV light escaping from the white LED is completely blocked and remarkably enhanced visible light extraction (400-750 nm) of the white LED which incorporated ODR packaging

was enhanced with an average enhancement of 15% in luminous intensity.

4.2 Sensing Devices

Like other metal oxides such as TiO_2 and zinc oxide (ZnO), Nb_2O_5 has shown great potential to be used as a sensing material. Sensor devices based on Nb_2O_5 for gas, humidity, biological and chemical sensing as well as photodetection have been successfully demonstrated. Generally, the main parameters for good sensing device performance are the size, morphology, aspect ratio, intergranular connectivity, porosity, surface energy, stoichiometry and surface area to volume ratio of the incorporated sensing material[205, 206].

In 1983, Kondo *et al.* reported the first Nb_2O_5 gas sensors for O_2 [207]. Before the nanostructured form of Nb_2O_5 had been introduced in a gas sensor, generally techniques such as RF magnetron sputtering was used to deposit dense Nb_2O_5 films [15, 208-210]. Several studies applied metal catalysts such as platinum (Pt) and palladium (Pd) onto the surface of Nb_2O_5, which could promote chemical reactions between the target gas and the oxide film and consequently, increase the sensing capability [55, 211, 212]. The types of sensing methods or principles that have so far been reported were mainly based on conductometric, voltammetric, chronoamperometric and Schottky contact sensors [15, 55, 208, 209, 211-220] Depending on the type of gas species, reducing or oxidizing, the interaction between the gas molecules and the Nb_2O_5 films changes the charge carrier concentration and the potential barrier of the Nb_2O_5 films. These affect the physio-chemical property of the films corresponding to the gas constituents exposed to the sensor. So far, the investigated gases that have been examined using Nb_2O_5 are O_2, hydrogen (H_2), dissolved O_2, carbon monoxide (CO), ammonia (NH_3) and a number of hydrocarbons (HCs) [15, 55, 208, 209, 211-220]. An example of a H_2 Schottky based gas sensor based on a Nb_2O_5/Pt contact and the dynamic responses of this device is presented in Figure 10. For humidity sensing, pellet type Nb_2O_5 sensors have been explored by Yadav *et al.* [221]. More recently, Fiz *et al.* have synthesized single-crystalline Nb_2O_5 nanorods and SnO_2/Nb_2O_5 core-shell heterostructures by CVD method [163]. The results have demonstrated that the growth of the nanoscopic Nb_2O_5 overlayer on SnO_2 nanowires introduced defects in the structure, which influenced the electronic properties of the material and enabled the design of more efficient sensor.

Due to the chemical stability and corrosion resistance of Nb_2O_5, the material has also been explored for pH and ascorbic acid measurements[5, 222]. Furthermore, Nb_2O_5 has also been used as a working electrode in electrochemical based DNA biosensors[223, 224].

Beside gas, chemical and biological sensing, it has been demonstrated that Nb_2O_5 with its wide bandgap and long electron life time, is a good candidate for making fast ultraviolet photodetection systems[225]. Fang *et al.* have shown that a photodetector based on individual Nb_2O_5 nanobelts resulted in a high external quantum-efficiency (EQE) of > 6000% [226].

4.3 Batteries and Supercapacitors

The development of energy storage devices based on lithium-ion batteries (LIBs) and supercapacitors have created great interest among researchers and Nb_2O_5 is certainly a favorable material for creating such storage devices[227-230]. Developing devices that can store sustainable energy with long term stability, very prolonged cycle life and meeting environmental constraints as well as safe operating potential windows (in the range of $1.0 \leq V \leq 3.0$ V vs. Li^+/Li) are the main goals of this field.

The study of Nb_2O_5 as an electrode material for lithium ion cells started in the early 1980s[231, 232]. The observations by Reichman *et al.* demonstrated that Nb_2O_5 can undergo intercalation with Li^+, leading to the possibility of repeated charging and discharging [231]. Subsequently, a LIB based on a Nb_2O_5 cathode was studied extensively by the Kumagai group [183, 232-239]. The structural changes of the Nb_2O_5 cathodes which are caused by discharging and recharging were investigated using X-ray photoelectron spectroscopy (XPS), X-ray diffraction (XRD) and X-ray absorption fine structure (XAFS) analysis methods[183, 232]. They suggested that tetragonal-Nb_2O_5 exhibited the best cycling performance with a large discharge capacity of 190 mAh g^{-1} for up to 30 cycles. XRD analysis suggested that the orthorhombic- and tetragonal-Nb_2O_5 maintain their original crystal lattices, accompanying a small change in the cell volume even after Li^+ intercalation. However, the two-dimensional layered structure of tetragonal-Nb_2O_5 was suggested to be the best for accommodating a large concentration of the intercalating ions [183]. Investigations of Nb_2O_5 LIBs using several electrolytes and different amounts of graphite in the electrodes have also been reported [239]. It was observed that the discharge capacity decreased with a decrease in the graphite content, and declined to 20 - 120 mAh per gram oxide in the graphite content range 0 - 10 wt.%. Furthermore, there are also reports on the application of sputtered Nb_2O_5 as a LIB electrode (Figure 11a and b)[236, 238]. Nakazawa *et al.* reported a battery with a sputtered Nb_2O_5 negative electrode of 100 nm thickness showed the most favourable charge-discharge properties with a capacity of 310 – 380 mAh cm^{-3} for 500 cycles[238].

Obviously the incorporation of nanostructured Nb_2O_5 should enhance the performance of LIBs. Nb_2O_5 nanobelts were the first nanostructured Nb_2O_5 to be used as an electrode material in LIBs which reported a potential window of 3.0-1.2 V (*vs.* Li^+/Li) [240]. LIBs made of Nb_2O_5 nanobelts demonstrated a high reversible charge/discharge capacity, high rate capability with excellent cycling stability as large as 180 $mAhg^{-1}$ after 50 cycles which could work smoothly even at a high current density of 10 Ag^{-1}. Le Viet *et al.* reported LIBs based on three different polymorphs of Nb_2O_5 nanofibers prepared by an electrospinning method and annealing treatment [31]. Among pseudohexagonal-, orthorhombic- and monoclinic-Nb_2O_5 nanofibers, the monoclinic based LIB showed the highest capacity, lowest capacity fading and good cycling stability. In addition, Li *et al.* demonstrated that Nb_2O_5 nanocrystals coated with a thin layer of a homogeneous carbon shell as an electrode demonstrated a relatively long cycle life (130 $mAhg^{-1}$ after over 300 cycles) by preventing the Nb_2O_5 volume change and pulverization during the charge-discharge process[87]. A study on Ta-substituted Nb_2O_5 nanofibers and Nb_2O_5 nanocomposites with various vanadium oxide contents - based LIBs have also been discussed elsewhere [119, 241]. A report on a battery based on a Nb_2O_5 anode with a KS-6 graphite cathode showed it to be an inherently safe energy storage system due to no oxygen release from the cathode materials, no lithium dendrite formation and no possibility of overcharge from the electrode/electrolyte reaction [242]. However, the cell capacity and cycling stability of such devices are still considered to be low.

Sasidharan *et al.* demonstrated a LIB based on Nb_2O_5 hollow nanospheres which can deliver a high capacity of 172 $mAhg^{-1}$ after 250 cycles of charge/discharge that maintained electrode structural integrity with an excellent cycling stability even after exposing it to a high current density of 6.25 Ag^{-1} [24]. In this work, the enhanced LIB's performance was attributed to the hollow cavity coupled with the nanosized Nb_2O_5 shell domain that facilitated fast lithium intercalation/deintercalation kinetics. Meanwhile, anodic Nb_2O_5 electrodes for LIB applications have been reported by Yoo *et al.* [102]. The discharge capacity of 53 μAh cm^{-2} was obtained at 800 nm thick Nb_2O_5 without a surface dissolution layer at a potential window of 1.2 – 3.0 V. Experiments were also conducted by Rahman *et al.* using LIB electrodes based on vein-like nanoporous networks of anodic Nb_2O_5 mixed with acetylene carbon black[103]. The device exhibited a reversible capacity of 175 $mAhg^{-1}$ even after 300 cycles at a current density of 0.4 Ag^{-1} and a potential window of 1.2-3.0 V (Figure 11c and d). This work also demonstrated an excellent reversible discharge capacity at a high current density of 2.6 Ag^{-1}.

In comparison to batteries, supercapacitors (SCs) offer significantly higher power densities with longer cycling life and fast charging. However, the main shortcoming of SCs is their low energy density, due to the restricted storage capacity as a result of the limitation of the size of the electrodes. One possible strategy to address these challenges is to develop high energy density electrodes. The effect of Nb_2O_5 crystallinity on the capacitive response of SCs has been reported by Kim *et al.* [243]. Augustyn *et al.* have shown that thick electrodes of up to 40 μm offer the promise of exploiting intercalation pseudocapacitance to obtain high-rate charge-storage devices[244]. Another study on understanding the origin of high-rate intercalation pseudocapacitance in Nb_2O_5 crystals was presented by Lubimtsev *et al.* [245].

So far, incorporation of carbon with Nb_2O_5 to fabricate a composite SC electrode has been considered as one of the most effective solutions in developing high energy density electrodes [246]. Wang *et al.* developed a SC electrode that consisted of CNT networks intimately mixed with Nb_2O_5 nanocrystals to generate a SC with a high capacitance, excellent rate capability as well as cycling capability [247]. The intimate contact between the nanocrystals and the CNTs enabled fast electron transport and increased current, while the small dimensions of the nanocrystals shortened the lithium-ion diffusion length.

4.4 Catalysts

Nb_2O_5 in its pure form has been used as a high temperature catalyst for the oxidative dehydrogenation (ODH) of organic materials in their gaseous form such as methane to formaldehyde and propane to propene[28, 248]. In addition, other reports have demonstrated that Nb_2O_5 could serve as an efficient catalyst for the transesterification of β-keto esters with several kinds of alcohols, leading to good conversion at acceptable yields [249]. It has been suggested that the catalytic performance of each polymorphic form of Nb_2O_5 differs significantly from one another. However, Nb_2O_5 has commonly been used with other metal oxides/metals due to the following properties that it offers to the composite catalyst [250-252]: (i) promotion and support properties: Nb_2O_5 enhances catalytic activity, selectivity and prolongs catalyst life when a small amount of this oxide is added to known catalysts, (ii) acidic property: the surface acid strength of hydrated Nb_2O_5 exhibits high catalytic activity, selectivity and stability for acid catalysed reactions in which water molecules participate, and (iii) redox properties and photosensitivity: Nb_2O_5 in mixed oxides is an oxidant and demonstrates photosensitivity.

Similar to its pure form, Nb_2O_5 has also been used together with other metal/metal oxide for the dehydrogenation of organic compounds in their gaseous forms[250, 251, 253-255]. Cherian *et al.* investigated a Nb_2O_5 supported chromium oxide (Cr_2O_3) catalyst for the ODH of propane to propene which demonstrated more than 80% selectivity in a temperature range of 673-723 K [254]. They also claimed the Nb_2O_5 support did not degrade the propene as much as Al_2O_3 and TiO_2 supports. The ODH of propane was also investigated by the addition of 1 to 20 wt % of Nb_2O_5 in Pd/Al_2O_3 catalysts (Figure 12) [256]. Similar catalytic properties have also been shown for other metal oxide compounds with Nb_2O_5 including Re_2O_7, CrO_3, WO_3, MoO_3, and V_2O_5 [257].

Nb_2O_5 has also been utilised as a photocatalyst. Under illumination, Nb_2O_5 produces electron/hole pairs that can generate hydroxyl radicals (•HO) from water, which are able to undergo further reactions in solution. Such photocatalytic applications have been successfully demonstrated for water splitting and degradation of harmful organic contaminants[47, 89, 258-263]. Increased photocatalytic activity was achieved by forming Nb_2O_5 nanostructures such as mesoporous, electrospun nanofibers, nanorods and nanospheres as a result of their high surface area[258, 262]. The addition of metal particles (i.e., Pt, Au, Cu) and metal oxides (i.e., CuO, NiO) into a Nb_2O_5 photocatalysts can delay the electron and hole recombination rate which enhances reduction reactions and improves the hydrogen production rate[259, 260]. Furthermore, carbon incorporation is also an effective technique to enhance photocatalytic activity. This is due to the capability of the carbon to modify the surface chemical composition of Nb_2O_5 and extend its absorption into the visible light range [262].

4.5 Electrochromic Devices

Electrochromism is the ability of a material to change its transparency upon exposure to stimuli. Electrochromic (EC) materials are at the core of a variety of applications including smart windows for architectural and automotive industries as well as optical displays[264-266]. An ideal EC material should have high initial transparency, large optical contrast between coloured and bleach states, short switching time, and long-term cyclic stability [267].

Nb_2O_5 has an excellent potential for the development of EC systems. It has multicolour capabilities and it also shows long-term cyclic stability due to its relatively large band gap [268, 269]. To date, the best EC ever reported has been for elevated temperature anodized Nb_2O_5 showing values as large as 47.0 cm^2 C^{-1} at an applied potential of −1.5 V for samples of 500 nm thickness (Figure 13) [69]. Other studies of EC systems based on Nb_2O_5 films using other synthesis techniques including sol-gel, thermal oxidation, chemical vapour deposition and pulse-laser deposition have also been reported elsewhere but resulted in lower ECs [16, 29, 67, 118, 153, 269-272].

4.6 Other Applications

Nb_2O_5 has also been reported for applications other than those presented in sections 4.1 to 4.5. As highlights, Nb_2O_5 has been incorporated in electronic devices such as memristors, capacitors, and field-effect transistors (FETs).

Highly crystalline orthorhombic Nb_2O_5 nanofibers obtained by electrospinning have been used in the development of memristors [273]. Reproducible bipolar resistive switching with an ON-OFF resistance ratio as high as 2×10^4 was observed in individual fibers. Hota *et al.* investigated the performance of Pd nano-dots (NDs) embedded in Nb_2O_5 memristors by scanning tunnelling microscopy[30]. From the current-voltage measurements, the memristors showed non-volatile memory and bipolar resistive switching characteristics. They claimed that the inclusion of Pd NDs played a critical role by acting as oxygen ion reservoirs and/or by polarizing a large volume of oxygen vacancies[30]. In addition, non-volatile resistive switching behaviour was also demonstrated at anodic Nb_2O_5 based memristors (in the configuration of Au/ Nb_2O_5/Nb/Si sandwich memory cells)[274]. The devices exhibited reproducible performance with a resistance ON-OFF ratio of $\sim10^3$.

Meanwhile, an interesting report on a capacitor based on Nb_2O_5 was presented by Garcia *et al.*, who investigated the influence of the growth and annealing temperatures on the electrical properties of Nb_2O_5 based MIM capacitors[64]. The obtained results show that the permittivity values exceeded 50 for the films crystallized after annealing at temperatures higher than 500 °C. However, the leakage current values for the crystalline films were higher than those in the case of amorphous films.

It has also been shown recently that Nb_2O_5 can be used in FETs by Kao *et. al.* [275]. The gain of the device could be readily controlled via the gate voltage modulations. The same group also showed the incorporation of such a FET as transducers for pH and biosensing.

Conclusion and Future Outlook

In this comprehensive review, we have presented the fundamental physical and chemical properties of Nb_2O_5, focusing on crystal structure and its electrical, optical, mechanical and thermal properties. In addition, we also discussed the various techniques that have been used to synthesize various forms of Nb_2O_5, and the most commonly reported applications incorporating Nb_2O_5 were summarized.

It was highlighted that Nb_2O_5 is found in a variety of crystal phases. The most common phases that are observed include pseudohexagonal, orthorhombic and monoclinic. There are still many unsubstantiated statements regarding the crystal structures of Nb_2O_5, especially when sub stoichiometry is present, thus more rigorous crystal phase analysis should be conducted to shed light on such conflicting arguments. Tetragonal Nb_2O_5, which is an unstable crystal structure between the orthorhombic and monoclinic phases, is still not well understood and less explored, which may present an opportunity for future research.

The reports regarding band energy diagrams, and as a result, the electronic and optical properties of Nb_2O_5 were presented. The mechanical and thermal properties of Nb_2O_5 were also discussed. However, it was hinted that many fundamental topics such as the Seebeck coefficient, thermal conductivity and carrier mobility of Nb_2O_5 have been rarely studied opening great avenues for future investigations.

Numerous synthesis techniques of Nb_2O_5 were briefly discussed in this review. It was seen that there exists a wide range of nanostructured Nb_2O_5 that have been successfully synthesized including nanoporous, nanosheets, nanorods, nanochannels, and nanowires, among others. However, a variety of other Nb_2O_5 morphologies have yet to be explored and fully characterized. We also believe that simple synthesis methods and low cost production routes should be investigated in more detail.

We have described numerous applications of Nb_2O_5 in catalysis, electrochromic devices, batteries, sensors and solar cells. However, many of these studies are still in their infancy and require further exploration. For example, in solar cell applications, Nb_2O_5 has received relatively little attention compared to materials such as TiO_2 and ZnO even though theoretically, Nb_2O_5 in both dye sensitized and heterostructure systems can offer enhanced efficiency. Furthermore, Nb_2O_5 in transistor, memristor and superconductor devices has been less studied compared to other metal oxides. There are certainly significant chances for further investigations of the capabilities of these devices through the exploitation of nanostructured Nb_2O_5.

Since Nb_2O_5 demonstrates excellent mechanical flexibility and durability as well as fantastic electronic and optical properties, one should consider the opportunity for its use in microelectro-mechanical systems (MEMS) and sensors, especially in combination with microfluidics and biomedical devices. There are many more applications that can be considered and comprehensive studies using Nb_2O_5 in many relevant fields should be encouraged, since its capability in many applications has not yet been examined.

Notes and references

[a]School of Electrical and Computer Engineering, RMIT University, Melbourne, VIC 3001, Australia.

*Emails: rozina.abdulrani@student.rmit.edu.au and kourosh.kalantar@rmit.edu.au

[b]Faculty of Electrical Engineering, Universiti Teknologi MARA, 40450 Shah Alam, Malaysia.

[c]School of Chemistry, Physics and Mechanical Engineering, Queensland University of Technology, GPO Box 2434, Brisbane, QLD, 4001, Australia.

1. F. Holtzberg, A. Reisman, M. Berry and M. Berkenblit, *Journal of the American Chemical Society*, 1957, 79, 2039-2043.
2. G. Brauer, *Zeitschrift Fur Anorganische Und Allgemeine Chemie*, 1941, 248, 1-31.
3. H. Schäfer, R. Gruehn and F. Schulte, *Angewandte Chemie International Edition in English*, 1966, 5, 40-52.
4. M. P. F. Graca, A. Meireles, C. Nico and M. A. Valente, *Journal of Alloys and Compounds*, 2013, 553, 177-182.
5. L. T. Arenas, P. C. M. Villis, J. Arguello, R. Landers, E. V. Benvenutti and Y. Gushikem, *Talanta*, 2010, 83, 241-248.
6. D. Velten, E. Eisenbarth, N. Schanne and J. Breivie, *Journal of Materials Science-Materials in Medicine*, 2004, 15, 457-461.
7. R. Pinto and B. M. Shaha, *Japanese Journal of Applied Physics*, 1968, 7, 1542.
8. B. Lelevic, N. Fuschillo and N. K. Annamalai, *Thin Solid Films*, 1974, 23, 249-256.
9. P. Griesmar, G. Papin, C. Sanchez and J. Livage, *Chemistry of Materials*, 1991, 3, 335-339.
10. G. R. Lee and J. A. Crayston, *Journal of Materials Chemistry*, 1991, 1, 381-386.

11. N. Machida, M. Tatsumisago and T. Minami, *Journal of the Electrochemical Society*, 1986, 133, 1963-1966.
12. E. I. Ko, J. M. Hupp and N. J. Wagner, *Journal of the Chemical Society-Chemical Communications*, 1983, 94-95.
13. K. Kunimori, H. Abe and T. Uchijima, *Chemistry Letters*, 1983, 1619-1622.
14. A. V. Chadwick, W. Zhou and J. M. Thomas, *Angewandte Chemie-International Edition in English*, 1989, 28, 75-76.
15. D. Rosenfeld, P. E. Schmid, S. Széles, F. Lévy, V. Demarne and A. Grisel, *Sens. Actuators, B*, 1996, 37, 83-89.
16. M. A. B. Gomes, L. O. d. S. Bulhões, S. C. de Castro and A. J. Damião, *Journal of The Electrochemical Society*, 1990, 137, 3067-3070.
17. M. A. Aegerter, M. Schmitt and Y. P. Guo, *International Journal of Photoenergy*, 2002, 4, 1-10.
18. Ö. D. Coşkun and S. Demirela, *Applied Surface Science*, 2013, 277, 35-39.
19. M. Kovendhan, D. P. Joseph, P. Manimuthu, S. Ganesan, S. Sambasivam, P. Maruthamuthu, S. A. Suthanthiraraj, C. Venkateswaran and R. Mohan, *Transactions of the Indian Institute of Metals*, 2011, 64, 185-188.
20. R. Ghosh, M. K. Brennaman, T. Uher, M.-R. Ok, E. T. Samulski, L. E. McNeil, T. J. Meyer and R. Lopez, *Acs Applied Materials & Interfaces*, 2011, 3, 3929-3935.
21. C. Nico, L. Rino, M. Matos, R. Monteiro, F. M. Costa, T. Monteiro and M. P. F. Graça, *Journal of the European Ceramic Society*, 2013, 33, 3077-3083.
22. R. Abdul Rani, A. S. Zoolfakar, J. Subbiah, J. Z. Ou and K. Kalantar-zadeh, *Electrochemistry Communications*, 2014, 40, 20-23.
23. J. Z. Ou, R. A. Rani, M. H. Ham, M. R. Field, Y. Zhang, H. Zheng, P. Reece, S. Zhuiykov, S. Sriram, M. Bhaskaran, R. B. Kaner and K. Kalantar-Zadeh, *ACS Nano*, 2012, 6, 4045-4053.
24. M. Sasidharan, N. Gunawardhana, M. Yoshio and K. Nakashima, *Materials Research Bulletin*, 2012, 47, 2161-2164.
25. K. Kamada, M. Mukai and Y. Matsumoto, *Electrochimica Acta*, 2004, 49, 321-327.
26. S. Abe, *Nanoscale Research Letters*, 2012, 7, 1-6.
27. A. Le Viet, R. Jose, M. V. Reddy, B. V. R. Chowdari and S. Ramakrishna, *Journal of Physical Chemistry C*, 2010, 114, 21795-21800.
28. B. Michalkiewicz, J. Srenscek-Nazzal, P. Tabero, B. Grzmil and U. Narkiewicz, *Chemical Papers*, 2008, 62, 106-113.
29. A. Michel A, *Solar Energy Materials and Solar Cells*, 2001, 68, 401-422.
30. M. K. Hota, M. K. Bera, S. Verma and C. K. Maiti, *Thin Solid Films*, 2012, 520, 6648-6652.
31. A. L. Viet, M. V. Reddy, R. Jose, B. V. R. Chowdari and S. Ramakrishna, *J. Phys. Chem. C* 2009, 114, 664-671.
32. I. N. a. M. Ziolek, *Chem. Rev.*, 1999, 99, 3603-3624.
33. L. A. Reznichenko, V. V. Akhnazarova, L. A. Shilkina, O. N. Razumovskaya and S. I. Dudkina, *Crystallography Reports*, 2009, 54, 483-491.
34. E. I. Ko and J. G. Weissman, *Catalysis Today*, 1990, 8, 27-36.
35. W. Mertin, S. Andersson and R. Gruehn, *Journal of Solid State Chemistry*, 1970, 1, 419-424.
36. E. Tsang, X. Zhou, L. Ye and S. C. Edman Tsang, *Nano Reviews*, 2012, 3, 17631.
37. Y. Kobayashi, H. Hata, M. Salama and T. E. Mallouk, *Nano Letters*, 2007, 7, 2142-2145.
38. H. Zhang, Y. Wang, D. Yang, Y. Li, H. Liu, P. Liu, B. J. Wood and H. Zhao, *Advanced Materials*, 2012, 24, 1598-1603.
39. J. S. Anderson, J. M. Browne and J. L. Hutchison, *Nature*, 1972, 237, 151-153.
40. T. Ikeya and M. Senna, *Journal of Non-Crystalline Solids*, 1988, 105, 243-250.
41. H. Luo, W. Song, P. G. Hoertz, K. Hanson, R. Ghosh, S. Rangan, M. K. Brennaman, J. J. Concepcion, R. A. Binstead, R. A. Bartynski, R. Lopez and T. J. Meyer, *Chemistry of Materials*, 2012, 25, 122-131.
42. J. W. Schultze and M. M. Lohrengel, *Electrochimica Acta*, 2000, 45, 2499-2513.
43. T. Proslier, J. Zasadzinski, L. Cooley, M. Pellin, J. Norem, J. Elam, C. Z. Antoine, R. A. Rimmer and P. Kneisel, *Applied Superconductivity, IEEE Transactions on*, 2009, 19, 1404-1408.
44. S. Zhuiykov and E. Kats, *World Academy of Science, Engineering and Technology*, 2013, 78.
45. A. D. Yoffe, *Advances in Physics*, 2002, 51, 799-890.
46. K. Sattler, *The energy gap of clusters, nanoparticles, and quantum dots*, Academic Press, New York 2002.
47. A. Esteves, L. C. A. Oliveira, T. C. Ramalho, M. Goncalves, A. S. Anastacio and H. W. P. Carvalho, *Catalysis Communications*, 2008, 10, 330-332.
48. J. Liu, D. Xue and K. Li, *Nanoscale Research Letters*, 2011, 6.
49. R. Brayner and F. Bozon-Verduraz, *Physical Chemistry Chemical Physics*, 2003, 5, 1457-1466.
50. G. Agarwal and G. B. Reddy, *Journal of Materials Science: Materials in Electronics*, 2005, 16, 21-24.
51. M. Palatnikov, O. Shcherbina, N. Sidorov and K. Bormanis, *Ukrainian Journal of Physical Optics*, 2012, 13.
52. L. K. Frevel and H. W. Rinn, *Analytical Chemistry*, 1955, 27, 1329-1330.
53. O. Kubaschewski and B. E. Hopkins, *Journal of the Less Common Metals*, 1960, 2, 172-180.
54. W. T. Holser, *Acta Crystallographica*, 1956, 9, 196-196.
55. Z. Wang, Y. Hu, W. Wang, X. Zhang, B. Wang, H. Tian, Y. Wang, J. Guan and H. Gu, *Int. J. Hydrogen Energy* 2012, 37, 4526-4532.
56. R. Norin and A. Magnéli, *Naturwissenschaften*, 1960, 47, 354-355.
57. B. M. Gatehouse and A. D. Wadsley, *Acta Crystallographica*, 1964, 17, 1545-1554.
58. K. Kato, *Acta Crystallographica Section B*, 1976, 32, 764-767.
59. S. Aggarwal and R. Ramesh, *Annual Review of Materials Science*, 1998, 28, 463-499.
60. E. H. Greener, D. H. Whitmore and M. E. Fine, *The Journal of Chemical Physics*, 1961, 34, 1017-1023.
61. P. Kofstad, *Journal of Physics and Chemistry of Solids*, 1962, 23, 1571.
62. W. K. Chen and R. A. Swalin, *Journal of Physics and Chemistry of Solids*, 1966, 27, 57-64.
63. S. Clima, G. Pourtois, S. Van Elshocht, S. De Gendt, M. M. Heyns, D. J. Wouters and J. A. Kittl, *ECS Transactions*, 2009, 19, 729-737.

64. H. García, H. Castán, E. Perez, S. Dueñas, L. Bailón, T. Blanquart, J. Niinistö, K. Kukli, M. Ritala and M. Leskelä, *Semiconductor Science and Technology*, 2013, 28, 055005.
65. G. E. Cavigliasso, M. J. Esplandiu and V. A. Macagno, *Journal of Applied Electrochemistry*, 1998, 28, 1213-1219.
66. J. Yahia, *Journal of Physics and Chemistry of Solids*, 1964, 25, 881-887.
67. A. Pawlicka, M. Atik and M. A. Aegerter, *Thin Solid Films*, 1997, 301, 236-241.
68. M. Schmitt, S. Heusing, M. A. Aegerter, A. Pawlicka and C. Avellaneda, *Solar Energy Materials and Solar Cells*, 1998, 54, 9-17.
69. D. D. Yao, R. A. Rani, A. P. O'Mullane, K. Kalantar-zadeh and J. Z. Ou, *The Journal of Physical Chemistry C*, 2014, 118, 476-481.
70. E. Çetinörgü-Goldenberg, J.-E. Klemberg-Sapieha and L. Martinu, *Applied Optics*, 2012, 51, 6498-6507.
71. C.-C. Lee, C.-L. Tien and J.-C. Hsu, *Applied Optics*, 2002, 41, 2043-2047.
72. N. Özer, M. D. Rubin and C. M. Lampert, *Solar Energy Materials and Solar Cells*, 1996, 40, 285-296.
73. X. Xiao, G. Dong, C. Xu, H. He, H. Qi, Z. Fan and J. Shao, *Appl. Surf. Sci.*, 2008, 255, 2192-2195.
74. O. B. Shcherbina, M. N. Palatnikov and V. V. Efremov, *Inorganic Materials*, 2012, 48, 433-438.
75. S. Park, G. Wang, B. Cho, Y. Kim, S. Song, Y. Ji, M.-H. Yoon and T. Lee, *Nat Nano*, 2012, 7, 438-442.
76. J. Lewis, *Materials Today*, 2006, 9, 38-45.
77. J. Hu, L. Li, H. Lin, P. Zhang, W. Zhou and Z. Ma, *Opt. Mater. Express*, 2013, 3, 1313-1331.
78. C. Peng, Z. Jia, H. Neilson, T. Li and J. Lou, *Advanced Engineering Materials*, 2013, 15, 250-256.
79. M. K. Hota, M. K. Bera and C. K. Maiti, *Semiconductor Science and Technology*, 2012, 27.
80. W. R. Manning, O. Hunter, F. W. Calderwood and D. W. Stacy, *Journal of the American Ceramic Society*, 1972, 55, 342-347.
81. D. L. Douglass, *Journal of the Less Common Metals*, 1963, 5, 151-157.
82. G. L. Dwivedi and E. C. Subbarao, *Journal of the American Ceramic Society*, 1973, 56, 443-444.
83. H. Choosuwan, R. Guo, A. S. Bhalla and U. Balachandran, *Journal of Applied Physics*, 2002, 91, 5051-5054.
84. M. N. Palatnikov, O. B. Shcherbina, A. A. Frolov, V. N. Pavlikov, M. V. Karpets, O. V. Makarova, N. V. Sidorov and V. T. Kalinnikov, *Inorganic Materials*, 2010, 46, 683-690.
85. K. E. Jesse, *Journal of Applied Physics*, 1969, 40, 3386-3389.
86. H. Luo, M. Wei and K. Wei, *Materials Chemistry and Physics*, 2010, 120, 6-9.
87. G. Li, X. Wang and X. Ma, *Journal of Energy Chemistry*, 2013, 22, 357-362.
88. O. F. Lopes, E. C. Paris and C. Ribeiro, *Applied Catalysis B: Environmental*, 2014, 144, 800-808.
89. Y. Zhao, C. Eley, J. Hu, J. S. Foord, L. Ye, H. He and S. C. E. Tsang, *Angewandte Chemie-International Edition*, 2012, 51, 3846-3849.
90. G. K. M. K. Shankar, H. E. Prakasam, S. Yoriya, M. Paulose, O. K. Varghese and C. A. Grimes, *Nanotechnology*, 2007, 18, 065707.
91. D. Regonini, C. R. Bowen, A. Jaroenworaluck and R. Stevens, *Materials Science and Engineering: R: Reports*, 2013, 74, 377-406.
92. P. H. G. Draper and J. Harvey, *Acta Metallurgica*, 1963, 11, 873-879.
93. G. C. Wood and C. Pearson, *Nature*, 1965, 208, 547-549.
94. M. R. Arora and R. Kelly, *Journal of Materials Science*, 1977, 12, 1673-1684.
95. A. Aladjem, D. G. Brandon, J. Yahalom and J. Zahavi, *Electrochimica Acta*, 1970, 15, 663-671.
96. H. Habazaki, Y. Oikawa, K. Fushimi, Y. Aoki, K. Shimizu, P. Skeldon and G. E. Thompson, *Electrochim. Acta* 2009, 54, 946-951.
97. J. H. L. Jinsub Choi, Jaeyoung Lee and Kyung Ja Kim, *Nanotechnol.*, 2007, 18.
98. J. Choi, J. H. Lim, S. C. Lee, J. H. Chang, K. J. Kim and M. A. Cho, *Electrochimica Acta*, 2006, 51, 5502-5507.
99. Y. Oikawa, T. Minami, H. Mayama, K. Tsujii, K. Fushimi, Y. Aoki, P. Skeldon, G. E. Thompson and H. Habazaki, *Acta Materialia*, 2009, 57, 3941-3946.
100. Q. Lu, T. Hashimoto, P. Skeldon, G. E. Thompson, H. Habazaki and K. Shimizu, *Electrochemical and Solid-State Letters*, 2005, 8, B17-B20.
101. I. Sieber, H. Hildebrand, A. Friedrich and P. Schmuki, *Electrochemistry Communications*, 2005, 7, 97-100.
102. J. E. Yoo, J. Park, G. Cha and J. Choi, *Thin Solid Films*, 2013, 531, 583-587.
103. M. M. Rahman, R. A. Rani, A. Z. Sadek, A. S. Zoolfakar, M. R. Field, T. Ramireddy, K. Kalantar-zadeh and Y. Chen, *J Mater Chem A*, 2013, 1, 11019-11025.
104. J. Zhao, X. Wang, R. Xu, Y. Mi and Y. Li, *Electrochemical and Solid-State Letters*, 2007, 10, C31-C33.
105. R. L. Karlinsey, *Electrochemistry Communications*, 2005, 7, 1190-1194.
106. R. L. Karlinsey, *Journal of Materials Science*, 2006, 41, 5017-5020.
107. S. Yang, Y. Aoki and H. Habazaki, *Applied Surface Science*, 2011, 257, 8190-8195.
108. W. Wei, K. Lee, S. Shaw and P. Schmuki, *Chem. Commun.*, 2012, *48*, 4244-4246.
109. K. Lee, Y. Yang, M. Yang and P. Schmuki, *Chemistry-a European Journal*, 2012, 18, 9521-9524.
110. R. A. Rani, A. S. Zoolfakar, J. Z. Ou, R. Ab Kadir, H. Nili, K. Latham, S. Sriram, M. Bhaskaran, S. Zhuiykov, R. B. Kaner and K. Kalantar-Zadeh, *Chemical Communications*, 2013, 49, 6349-6351.
111. S. Barredo-Damas, K. Lee, R. Kirchgeorg, R. Sánchez-Tovar and P. Schmuki, *ECS Electrochemistry Letters*, 2013, 2, C4-C6.
112. L. L. Hench and J. K. West, *Chemical Reviews*, 1990, 90, 33-72.
113. Markus Niederberger and N. Pinna, in *Metal Oxide Nanoparticles in Organic Solvents*, Springer London, 2009, ch. 2, pp. 7-18.
114. A. Pierre, in *Introduction to Sol-Gel Processing*, Springer US, 1998, vol. 1, ch. 1, pp. 1-9.
115. T. Olding, M. Sayer and D. Barrow, *Thin Solid Films*, 2001, 398, 581-586.
116. C. Alquier, M. T. Vandenborre and M. Henry, *Journal of Non-Crystalline Solids*, 1986, 79, 383-395.

117. N. Ozer, T. Barreto, T. Buyuklimanli and C. M. Lampert, *Solar Energy Materials and Solar Cells*, 1995, 36, 433-443.
118. P. R. Bueno, C. O. Avellaneda, R. C. Faria and L. O. S. Bulhoes, *Electrochimica Acta*, 2001, 46, 2113-2118.
119. G. Li, X. Wang, Z. Chen, X. Ma and Y. Lu, *Electrochimica Acta*, 2013, 102, 351-357.
120. L. Melo, C. O. Avellaneda and A. Pawlicka, *Molecular Crystals and Liquid Crystals*, 2002, 374, 101-106.
121. P. Guo and M. A. Aegerter, *Thin Solid Films*, 1999, 351, 290-294.
122. M. Ristic, S. Popovic and S. Music, *Materials Letters*, 2004, 58, 2658-2663.
123. D. A. de Barros Filho, P. P. Abreu Filho, U. Werner and M. A. Aegerter, *Journal of Sol-Gel Science and Technology*, 1997, 8, 735-742.
124. T. Sreethawong, S. Ngamsinlapasathian and S. Yoshikawa, *Materials Letters*, 2012, 78, 135-138.
125. M. H. Habibi and R. Mokhtari, *Journal of Inorganic and Organometallic Polymers and Materials*, 2012, 22, 158-165.
126. I. Zhitomirsky, *Journal of the European Ceramic Society*, 1999, 19, 2581-2587.
127. Z. I, *Materials Letters*, 1998, 35, 188-193.
128. J.-H. Jang, T.-Y. Kim, N.-J. Kim, C.-H. Lee, E.-M. Park, C. Park and S.-J. Suh, *Materials Science and Engineering: B*, 2011, 176, 1505-1508.
129. D. Yang, *Nanocomposite films for gas sensing, advances in nanocomposites - Synthesis, characterization and industrial applications*, InTech, 2011.
130. Y. K. Yap, *Physical Vapor Deposition, Encyclopedia of Nanotechnology: SpringerReference* Springer, Berlin Heidelberg, 2012.
131. F. Richter, H. Kupfer, P. Schlott, T. Gessner and C. Kaufmann, *Thin Solid Films*, 2001, 389, 278-283.
132. B. Hunsche, M. Vergöhl, H. Neuhäuser, F. Klose, B. Szyszka and T. Matthée, *Thin Solid Films*, 2001, 392, 184-190.
133. S. Venkataraj, R. Drese, O. Kappertz, R. Jayavel and M. Wuttig, *physica status solidi (a)*, 2001, 188, 1047-1058.
134. K. Yoshimura, T. Miki and S. Tanemura, *Journal of The Electrochemical Society*, 1997, 144, 2982-2985.
135. H. Mähne, L. Berger, D. Martin, V. Klemm, S. Slesazeck, S. Jakschik, D. Rafaja and T. Mikolajick, *Solid-State Electronics*, 2012, 72, 73-77.
136. J. M. Chappé, P. Carvalho, S. Lanceros-Mendez, M. I. Vasilevskiy, F. Vaz, A. V. Machado, M. Fenker, H. Kappl, N. M. G. Parreira, A. Cavaleiro and E. Alves, *Surface and Coatings Technology*, 2008, 202, 2363-2367.
137. A. Dhar and T. L. Alford, *Journal of Applied Physics*, 2012, 112.
138. F. Lai, M. Li, H. Wang, H. Hu, X. Wang, J. G. Hou, Y. Song and Y. Jiang, *Thin Solid Films*, 2005, 488, 314-320.
139. F. Lai, L. Lin, Z. Huang, R. Gai and Y. Qu, *Applied Surface Science*, 2006, 253, 1801-1805.
140. A. Pignolet, G. M. Rao and S. B. Krupanidhi, *Thin Solid Films*, 1995, 261, 18-24.
141. R. C. Lee and C. R. Aita, *Journal of Applied Physics*, 1991, 70, 2094-2103.
142. S. V. Zaitsev, Y. V. Gerasimenko, S. N. Saltykov, D. A. Khoviv and A. M. Khoviv, *Inorganic Materials*, 2011, 47, 412-416.
143. T. Maruyama and S. Arai, *Applied Physics Letters*, 1993, 63, 869-870.
144. L. Berger, H. Maehne, V. Klemm, A. Leuteritz, T. Mikolajick and D. Rafaja, *Applied Physics a-Materials Science & Processing*, 2012, 108, 431-437.
145. Y. Shao, K. Yi, M. Fang and J. Zhang, in *Pacific Rim Laser Damage 2011: Optical Materials for High Power Lasers*, eds. J. Shao, K. Sugioka and C. J. Stolz, 2012, vol. 8206.
146. G. Ramírez, S. E. Rodil, S. Muhl, D. Turcio-Ortega, J. J. Olaya, M. Rivera, E. Camps and L. Escobar-Alarcón, *Journal of Non-Crystalline Solids*, 2010, 356, 2714-2721.
147. H. Wender, P. Migowski, A. F. Feil, S. R. Teixeira and J. Dupont, *Coordination Chemistry Reviews*, 2013, 257, 2468-2483.
148. P. J. Kelly and R. D. Arnell, *Vacuum*, 2000, 56, 159-172.
149. C.-L. Tien, *Applied Surface Science*, 2010, 257, 481-486.
150. C. M. Cotell, S. Schiestel, C. A. Carosella, S. Flom, G. K. Hubler and D. L. Knies, *Nuclear Instruments and Methods in Physics Research Section B: Beam Interactions with Materials and Atoms*, 1997, 127–128, 557-561.
151. B. Reichman and A. J. Bard, *Journal of The Electrochemical Society*, 1980, 127, 241-242.
152. M. Vinnichenko, A. Rogozin, D. Grambole, F. Munnik, A. Kolitsch, W. Möller, O. Stenzel, S. Wilbrandt, A. Chuvilin and U. Kaiser, *Applied Physics Letters*, 2009, 95.
153. Z. W. Fu, J. J. Kong and Q. Z. Qin, *Journal of The Electrochemical Society*, 1999, 146, 3914-3918.
154. S. Hyunjun, C. Dooho, L. Dongsoo, S. Seo, L. Myong-Jae, Y. In-Kyeong and H. Hyunsang, *Electron Device Letters, IEEE*, 2005, 26, 292-294.
155. M. E. Gimon-Kinsel and K. J. Balkus Jr, *Microporous and Mesoporous Materials*, 1999, 28, 113-123.
156. K. L. Choy, *Progress in Materials Science*, 2003, 48, 57-170.
157. Y. Kuzminykh, A. Dabirian, M. Reinke and P. Hoffmann, *Surface and Coatings Technology*, 2013, 230, 13-21.
158. C. d. O. da Silveira, AF; de Campos, SD; de Campos, EA; Fraporti, AD *Surface Engineering* 2012 28 68-72
159. N. Hara, E. Takahashi, J. H. Yoon and K. Sugimoto, *Journal of the Electrochemical Society*, 1994, 141, 1669-1674.
160. J. P. Masse, H. Szymanowski, O. Zabeida, A. Amassian, J. E. Klemberg-Sapieha and L. Martinu, *Thin Solid Films*, 2006, 515, 1674-1682.
161. S. A. O'Neill, I. P. Parkin, R. J. H. Clark, A. Mills and N. Elliott, *Journal of Materials Chemistry*, 2003, 13, 2952-2956.
162. A. F. de Oliveira, C. B. da Silveira, S. D. de Campos, E. A. de Campos and E. Carasek, *Talanta*, 2005, 66, 74-79.
163. R. Fiz, F. Hernandez-Ramirez, T. Fischer, L. Lopez-Conesa, S. Estrade, F. Peiro and S. Mathur, *The Journal of Physical Chemistry C*, 2013, 117, 10086-10094.
164. W. Hu, Z. Liu, D. Tian, S. Zhang, Y. Zhao and K. Yao, *Journal of Wuhan University of Technology-Materials Science Edition*, 2009, 24, 245-248.
165. J. Buha, D. Arcon, M. Niederberger and I. Djerdj, *Physical Chemistry Chemical Physics*, 2010, 12, 15537-15543.
166. H. Kominami, K. Oki, M. Kohno, S.-i. Onoue, Y. Kera and B. Ohtani, *Journal of Materials Chemistry*, 2001, 11, 604-609.

167. M. Wei, Z. m. Qi, M. Ichihara and H. Zhou, *Acta Mater.*, 2008, 56, 2488-2494.
168. W. Hu, Y. Zhao, Z. Liu and Y. Zhu, *Nanotechnology*, 2007, 18.
169. H. Luo, M. Wei and K. Wei, *Journal of Nanomaterials*, 2009, 2009.
170. S. Kunjara Na Ayudhya, A. Soottitantawat, P. Praserthdam and C. Satayaprasert, *Materials Chemistry and Physics*, 2008, 110, 387-392.
171. C. C. Li, J. Dou, L. Chen, J. Lin and H. C. Zeng, *ChemCatChem*, 2012, 4, 1675-1682.
172. L. Fei and X. Dongfeng, *Physica Scripta*, 2010, 2010, 014074.
173. H. Wen, Z. Liu, J. Wang, Q. Yang, Y. Li and J. Yu, *Appl. Surf. Sci.*, 2011, 257, 10084-10088.
174. M. Liu and D. Xue, *Materials Research Bulletin*, 2010, 45, 333-338.
175. S. H. Mujawar, A. I. Inamdar, C. A. Betty, V. Ganesan and P. S. Patil, *Electrochim. Acta*, 2007, 52, 4899-4906.
176. J. Xia, N. Masaki, K. Jiang and S. Yanagida, *Journal of Photochemistry and Photobiology A: Chemistry*, 2007, 188, 120-127.
177. R. Romero, J. R. Ramos-Barrado, F. Martin and D. Leinen, *Surface and Interface Analysis*, 2004, 36, 888-891.
178. R. Romero, E. A. Dalchiele, F. Martín, D. Leinen and J. R. Ramos-Barrado, *Solar Energy Materials and Solar Cells*, 2009, 93, 222-229.
179. T. Rajesh, V. Binni, G. M. Subodh, T. Eng Soon and S. Chorng Haur, *Nanotechnology*, 2011, 22, 115202.
180. J. H. Lim and J. Choi, *Journal of Industrial and Engineering Chemistry*, 2009, 15, 860-864.
181. J. H. Kang, Y. Myung, J. W. Choi, D. M. Jang, C. W. Lee, J. Park and E. H. Cha, *Journal of Materials Chemistry*, 2012, 22, 8413-8419.
182. B. Varghese, S. C. Haur and C.-T. Lim, *The Journal of Physical Chemistry C*, 2008, 112, 10008-10012.
183. R. Kodama, Y. Terada, I. Nakai, S. Komaba and N. Kumagai, *Journal of The Electrochemical Society*, 2006, 153, A583-A588.
184. S. Choopun, N. Hongsith and E. Wongrat, *Metal-Oxide Nanowires by Thermal Oxidation Reaction Technique*, 2010.
185. G. Michael, *J. Photoch. Photobio. C*, 2003, *4*, 145-153.
186. L. Alibabaei, H. Luo, R. L. House, P. G. Hoertz, R. Lopez and T. J. Meyer, *J Mater Chem A*, 2013, 1, 4133-4145.
187. R. Jose, V. Thavasi and S. Ramakrishna, *J. Am. Ceram. Soc.*, 2009, *92*, 289-301.
188. K. Sayama, H. Sugihara and H. Arakawa, *Chem. Mater.*, 1998, 10, 3825-3832.
189. L. Hu, M. Wolf, M. Grätzel and Z. Jiang, *J. Sol-Gel Sci. Techn.*, 1995, 5, 219-226.
190. B.-Y. Jeong and E. H. Jung, *Metals and Materials International*, 2013, 19, 617-622.
191. J. Xia, N. Masaki, K. Jiang and S. Yanagida, *Chemical Communications*, 2007, 138-140.
192. J. Xia, N. Masaki, K. Jiang and S. Yanagida, *The Journal of Physical Chemistry C*, 2007, 111, 8092-8097.
193. T.-Y. Cho, K.-W. Ko, S.-G. Yoon, S. S. Sekhon, M. G. Kang, Y.-S. Hong and C.-H. Han, *Current Applied Physics*, 2013, 13, 1391-1396.
194. J. Kim, *Journal of Nanoscience and Nanotechnology*, 2011, 11, 7335-7338.
195. E. Barea, X. Xu, V. Gonzalez-Pedro, T. Ripolles-Sanchis, F. Fabregat-Santiago and J. Bisquert, *Energy & Environmental Science*, 2011, 4, 3414-3419.
196. A. Zaban, S. G. Chen, S. Chappel and B. A. Gregg, *Chemical Communications*, 2000, 2231-2232.
197. S. G. Chen, S. Chappel, Y. Diamant and A. Zaban, *Chemistry of Materials*, 2001, 13, 4629-4634.
198. M. Wu, X. Lin, W. Guo, Y. Wang, L. Chu, T. Ma and K. Wu, *Chemical Communications*, 2013, 49, 1058-1060.
199. X. Lin, M. Wu, Y. Wang, A. Hagfeldt and T. Ma, *Chemical Communications*, 2011, 47, 11489-11491.
200. M. K. Siddiki, S. Venkatesan and Q. Qiao, *Physical Chemistry Chemical Physics*, 2012, 14, 4682-4686.
201. O. Wiranwetchayan, Z. Liang, Q. Zhang, G. Cao and P. Singjai, *Materials Sciences and Applications*, 2011, 2, 1697-1701.
202. F. Lenzmann, in *Mesoporous, nanoparticulate films of Nb_2O_5 and ZrO_2 preparation and characterization.*, Switzerland, 2000.
203. T. W. Hickmott, *Journal of Applied Physics*, 1966, 37, 4380-4388.
204. J.-C. Su, C.-L. Lu and C.-W. Chu, *Applied Optics*, 2009, 48, 4942-4946.
205. G. Shen, P.-C. Chen, K. Ryu and C. Zhou, *Journal of Materials Chemistry*, 2009, 19, 828-839.
206. N. S. Harale, D. L. Kamble, M. G. Gang, V. K. Rao, J. H. Kim and P. S. Patil, *Materials Today*, 2013, 16, 452-453.
207. H. T. H. Kondo, T. Takeuchi, I. Igarashi, *Proc. 3rd Sensor Symp., Japan*, 1983, 185-190.
208. L. Chambon, C. Maleysson, A. Pauly, J. P. Germain, V. Demarne and A. Grisel, *Sens. Actuators, B*, 1997, 45, 107-114.
209. L. Chambon, A. Pauly, J. P. Germain, C. Maleysson, V. Demarne and A. Grisel, *Sens. Actuators, B*, 1997, 43, 60-64.
210. L. Chambon, J. P. Germain, A. Pauly, V. Demarne and A. Grisel, *Sensors and Actuators B: Chemical*, 1999, 60, 138-147.
211. R. A. Rani, A. S. Zoolfakar, J. Z. Ou, M. R. Field, M. Austin and K. Kalantar-zadeh, *Sensors and Actuators B-Chemical*, 2013, 176, 149-156.
212. T. Hyodo, J. Ohoka, Y. Shimizu and M. Egashira, *Sens. Actuators, B*, 2006, 117, 359-366.
213. L. Chevallier, E. Di Bartolomeo, M. L. Grilli, M. Mainas, B. White, E. D. Wachsman and E. Traversa, *Sensors and Actuators B: Chemical*, 2008, 129, 591-598.
214. L. Chevallier, E. Di Bartolomeo, M. L. Grilli and E. Traversa, *Sensors and Actuators B: Chemical*, 2008, 130, 514-519.
215. H. G. Moon, H. W. Jang, J.-S. Kim, H.-H. Park and S.-J. Yoon, *Sens. Actuators, B*, 2011, 153, 37-43.
216. T. Hyodo, H. Shibata, Y. Shimizu and M. Egashira, *Sens. Actuators, B*, 2009, 142, 97-104.
217. A. Kohli, C. C. Wang and S. A. Akbar, *Sensors and Actuators B: Chemical*, 1999, 56, 121-128.
218. L. Chevallier, E. Traversa and E. Di Bartolomeo, *Journal of The Electrochemical Society*, 2010, 157, J386-J391.
219. M. S. P. Francisco, W. S. Cardoso and Y. Gushikem, *Journal of Electroanalytical Chemistry*, 2005, 574, 291-297.
220. U. Cvelbar, K. Ostrikov, A. Drenik and M. Mozetic, *Appl. Phys. Lett.*, 2008, 92, 133505-133503.

221. B. C. Yadav and M. Singh, *Sensors Journal, IEEE*, 2010, 10, 1759-1766.
222. O. Korostynska, K. Arshak, E. Gill, A. Arshak and K. Kaneswaran, 2008.
223. J. P. Marco, K. B. Borges, C. R. T. Tarley, E. S. Ribeiro and A. C. Pereira, *Journal of Electroanalytical Chemistry*, 2013, 704, 159-168.
224. S. Rho, D. Jahng, J. H. Lim, J. Choi, J. H. Chang, S. C. Lee and K. J. Kim, *Biosensors and Bioelectronics*, 2008, 23, 852-856.
225. L. Sang, M. Liao and M. Sumiya, *Sensors*, 2013, 13, 10482-10518.
226. X. Fang, L. Hu, K. Huo, B. Gao, L. Zhao, M. Liao, P. K. Chu, Y. Bando and D. Golberg, *Adv. Funct. Mater.* , 2011, 21, 3907-3915.
227. V. Etacheri, R. Marom, R. Elazari, G. Salitra and D. Aurbach, *Energy & Environmental Science*, 2011, 4, 3243-3262.
228. M. V. Reddy, G. V. Subba Rao and B. V. R. Chowdari, *Chemical Reviews*, 2013, 113, 5364-5457.
229. K. Naoi, S. Ishimoto, J.-i. Miyamoto and W. Naoi, *Energy & Environmental Science*, 2012, 5, 9363-9373.
230. Y. Jing, Z. Zhou, C. R. Cabrera and Z. Chen, *J Mater Chem A*, 2014.
231. B. Reichman and A. J. Bard, *Journal of The Electrochemical Society*, 1981, 128, 344-346.
232. N. Kumagai, K. Tanno, T. Nakajima and N. Watanabe, *Electrochimica Acta*, 1983, 28, 17-22.
233. B. Kaplan, H. Groult, N. Kumagai, S. Komaba and F. Lantelme, *Electrochemistry*, 2001, 69, 592-597.
234. N. Kumagai, Y. Koishikawa, S. Komaba and N. Koshiba, *Journal of the Electrochemical Society*, 1999, 146, 3203-3210.
235. N. Kumagai, S. Komaba and N. Kumagai, in *New Materials for Batteries and Fuel Cells*, eds. D. H. Doughty, L. F. Nazar, M. Arakawa, H. P. Brack and K. Naoi, 2000, vol. 575, pp. 39-47.
236. N. Kumagai, Y. Tateshita, Y. Takatsuka, M. Baba, T. Ikeda and K. Tanno, *Journal of Power Sources*, 1995, 54, 175-179.
237. F. Lantelme, H. Groult and N. Kumagai, *Electrochimica Acta*, 2000, 45, 3171-3180.
238. H. Nakazawa, K. Sano, T. Abe, M. Baba and N. Kumagai, *Journal of Power Sources*, 2007, 174, 838-842.
239. N. Kumagai, I. Ishiyama and K. Tanno, *Journal of Power Sources*, 1987, 20, 193-198.
240. M. Wei, K. Wei, M. Ichihara and H. Zhou, *Electrochemistry Communications*, 2008, 10, 980-983.
241. A. Le Viet, M. V. Reddy, R. Jose, B. V. R. Chowdari and S. Ramakrishna, *Electrochimica Acta*, 2011, 56, 1518-1528.
242. G. Park, N. Gunawardhana, C. Lee, S.-M. Lee, Y.-S. Lee and M. Yoshio, *Journal of Power Sources*, 2013, 236, 145-150.
243. J. W. Kim, V. Augustyn and B. Dunn, *Advanced Energy Materials*, 2012, 2, 141-148.
244. V. Augustyn, J. Come, M. A. Lowe, J. W. Kim, P. L. Taberna, S. H. Tolbert, H. D. Abruna, P. Simon and B. Dunn, *Nat Mater*, 2013, 12, 518-522.
245. A. A. Lubimtsev, P. R. C. Kent, B. G. Sumpter and P. Ganesh, *J Mater Chem A*, 2013, 1, 14951-14956.
246. P.-C. Chen, G. Shen, Y. Shi, H. Chen and C. Zhou, *ACS Nano*, 2010, 4, 4403-4411.
247. X. Wang, G. Li, Z. Chen, V. Augustyn, X. Ma, G. Wang, B. Dunn and Y. Lu, *Advanced Energy Materials*, 2011, 1, 1089-1093.
248. R. H. H. Smits, K. Seshan and J. R. H. Ross, *Journal of the Chemical Society-Chemical Communications*, 1991, 558-559.
249. M. I. de Sairre, E. S. Bronze-Uhle and P. M. Donate, *Tetrahedron Letters*, 2005, 46, 2705-2708.
250. K. Tanabe, *Catalysis Today*, 2003, 78, 65-77.
251. K. Tanabe and S. Okazaki, *Applied Catalysis a-General*, 1995, 133, 191-218.
252. T. Ushikubo, *Catalysis Today*, 2000, 57, 331-338.
253. I. E. Wachs, Y. Chen, J. M. Jehng, L. E. Briand and T. Tanaka, *Catalysis Today*, 2003, 78, 13-24.
254. M. Cherian, M. S. Rao and G. Deo, *Catalysis Today*, 2003, 78, 397-409.
255. M. Ziolek, *Catalysis Today*, 2003, 78, 47-64.
256. F. B. Noronha, D. A. G. Aranda, A. P. Ordine and M. Schmal, *Catalysis Today*, 2000, 57, 275-282.
257. J. M. Jehng, A. M. Turek and I. E. Wachs, *Applied Catalysis a-General*, 1992, 83, 179-200.
258. X. Chen, T. Yu, X. Fan, H. Zhang, Z. Li, J. Ye and Z. Zou, *Applied Surface Science*, 2007, 253, 8500-8506.
259. H.-Y. Lin, H.-C. Yang and W.-L. Wang, *Catalysis Today*, 2011, 174, 106-113.
260. Y.-H. Pai and S.-Y. Fang, *Journal of Power Sources*, 2013, 230, 321-326.
261. S. Qi, R. Zuo, Y. Liu and Y. Wang, *Materials Research Bulletin*, 2013, 48, 1213-1217.
262. S. Ge, H. Jia, H. Zhao, Z. Zheng and L. Zhang, *Journal of Materials Chemistry*, 2010, 20, 3052-3058.
263. S.-q. Guo, X. Zhang, Z. Zhou, G.-d. Gao and L. Liu, *J Mater Chem A*, 2014, 2, 9236-9243.
264. R. Baetens, B. P. Jelle and A. Gustavsen, *Solar Energy Materials and Solar Cells*, 2010, 94, 87-105.
265. N. M. Rowley and R. J. Mortimer, *Science progress*, 2002, 85, 243-262.
266. J. J. Ho, C. Y. Chen, C. M. Huang, W. J. Lee, W. R. Liou and C. C. Chang, *Applied Optics*, 2005, 44, 6176-6180.
267. S. K. Deb, *Solar Energy Materials and Solar Cells*, 2008, 92, 245-258.
268. S. Heusing, D. L. Sun, J. Otero-Anaya and M. A. Aegerter, *Thin Solid Films*, 2006, 502, 240-245.
269. C. O. Avellaneda, A. Pawlicka and M. A. Aegerter, *Journal of Materials Science*, 1998, 33, 2181-2185.
270. T. Maruyama and T. Kanagawa, *Journal of The Electrochemical Society*, 1994, 141, 2868-2871.
271. N. Ozer and C. M. Lampert, *Solar Energy Materials and Solar Cells*, 1998, 54, 147-156.
272. A. Verma and P. K. Singh, *Indian Journal of Chemistry Section a-Inorganic Bio-Inorganic Physical Theoretical & Analytical Chemistry*, 2013, 52, 593-598.
273. A. M. Grishin, A. A. Velichko and A. Jalalian, *Applied Physics Letters*, 2013, 103.
274. T. V. Kundozerova, A. M. Grishin, G. B. Stefanovich and A. A. Velichko, *IEEE Trans. Electron Devices*, 2012, 59, 1144-1148.
275. C.-H. Kao, H. Chen, L.-T. Kuo, J.-C. Wang, Y.-T. Chen, Y.-C. Chu, C.-Y. Chen, C.-S. Lai, S. W. Chang and C. W. Chang, *Sensors and Actuators B-Chemical*, 2014, 194, 419-426.

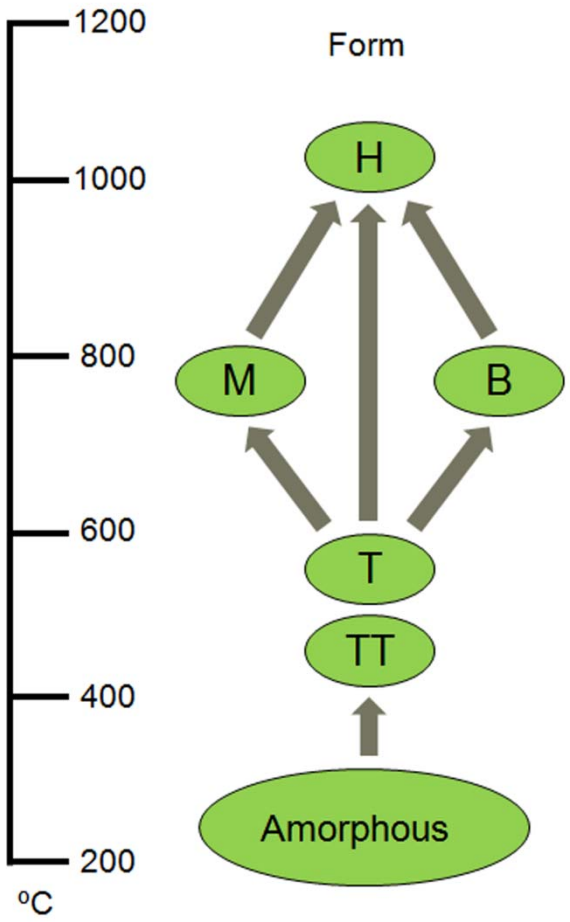

Figure 1: (a) Alteration of Nb_2O_5 crystal phase as a function of temperature. Reprinted with permission from ref. 34. Copyright 1990, Elsevier.

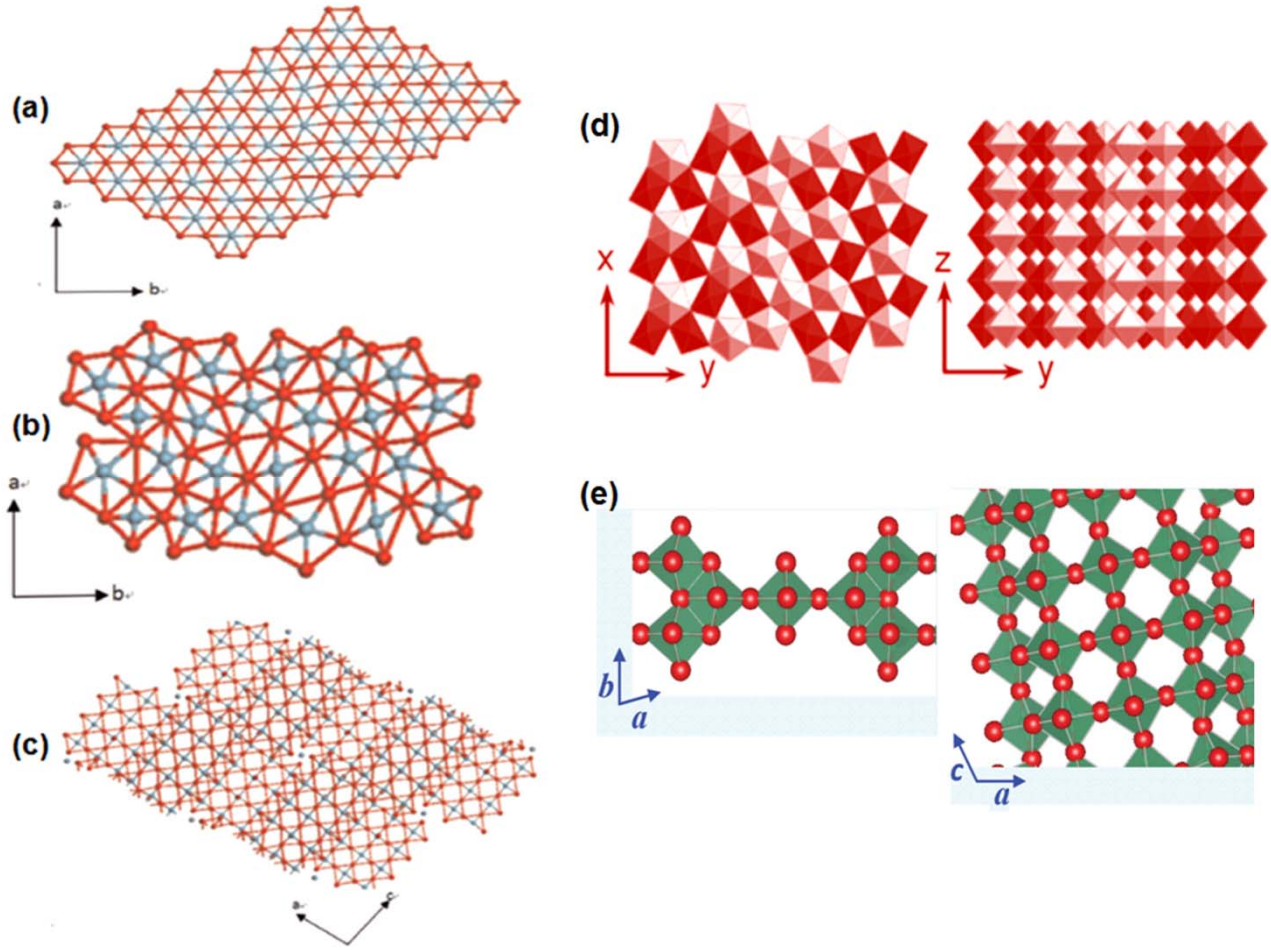

Figure 2: Atomic representation of (a) pseudohexagonal (TT-Nb_2O_5), (b) orthorhombic (T-Nb_2O_5), (c) monoclinic (H-Nb_2O_5) and 3D structure schematics of (d) orthorhombic (T-Nb_2O_5) and (d) monoclinic (H-Nb_2O_5). (a,b,c) Reprinted with permission from ref. 36. Copyright 2012, Co-Action Publishing, (d) Reprinted with permission from ref. 37. Copyright 2007, American Chemical Society, (e) Reprinted with permission from ref. 38. Copyright 2012, WILEY-VCH Verlag GmbH & Co. KGaA, Weinheim

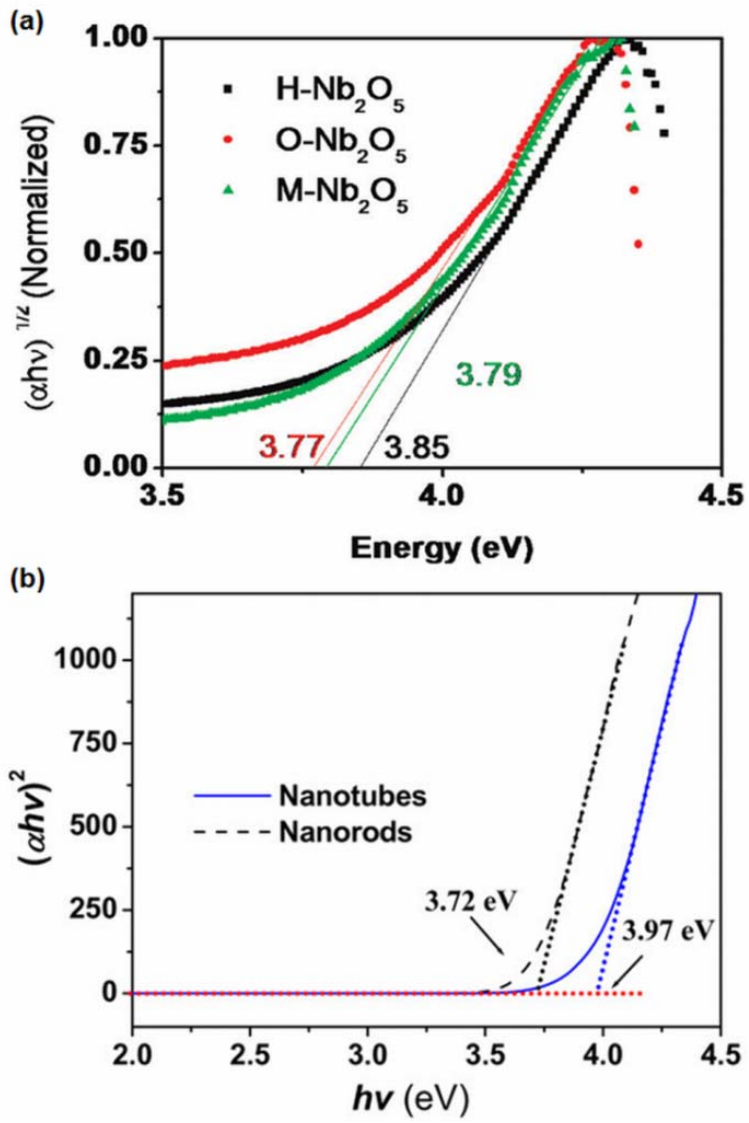

Figure 3: Tauc plot of $(\alpha h\nu)^2$ *vs*. photon energy ($h\nu$) of (a) hexagonal, orthorhombic and monoclinic Nb_2O_5 nanofibers, (b) orthorhombic Nb_2O_5 nanorods and nanotubes measured at room temperature. α is defined as absorption the coefficient. (a) Reprinted with permission from ref. 27. Copyright 2010, American Chemical Society, (b) Reprinted with permission from ref. 48. Copyright 2011, Springer.

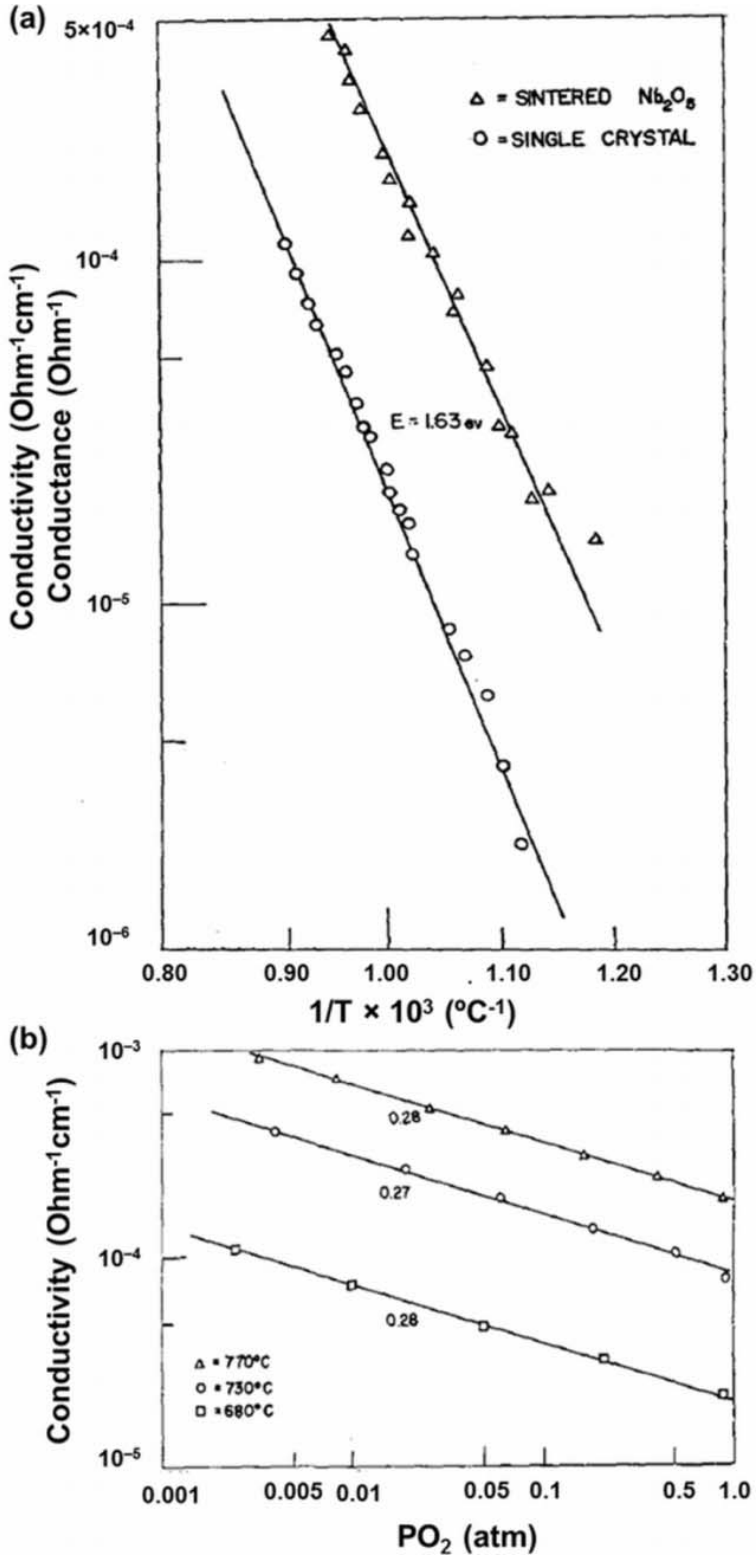

Figure 4: (a) Electrical conductivity of sintered α-Nb_2O_5 and electrical conductance of Nb_2O_5 single crystal versus 1/ *T* for specimens heated in air. (b) Electrical conductivity of sintered α-Nb_2O_5 versus oxygen partial pressure. Reprinted with permission from ref. 60. Copyright 1961, AIP Publishing LLC.

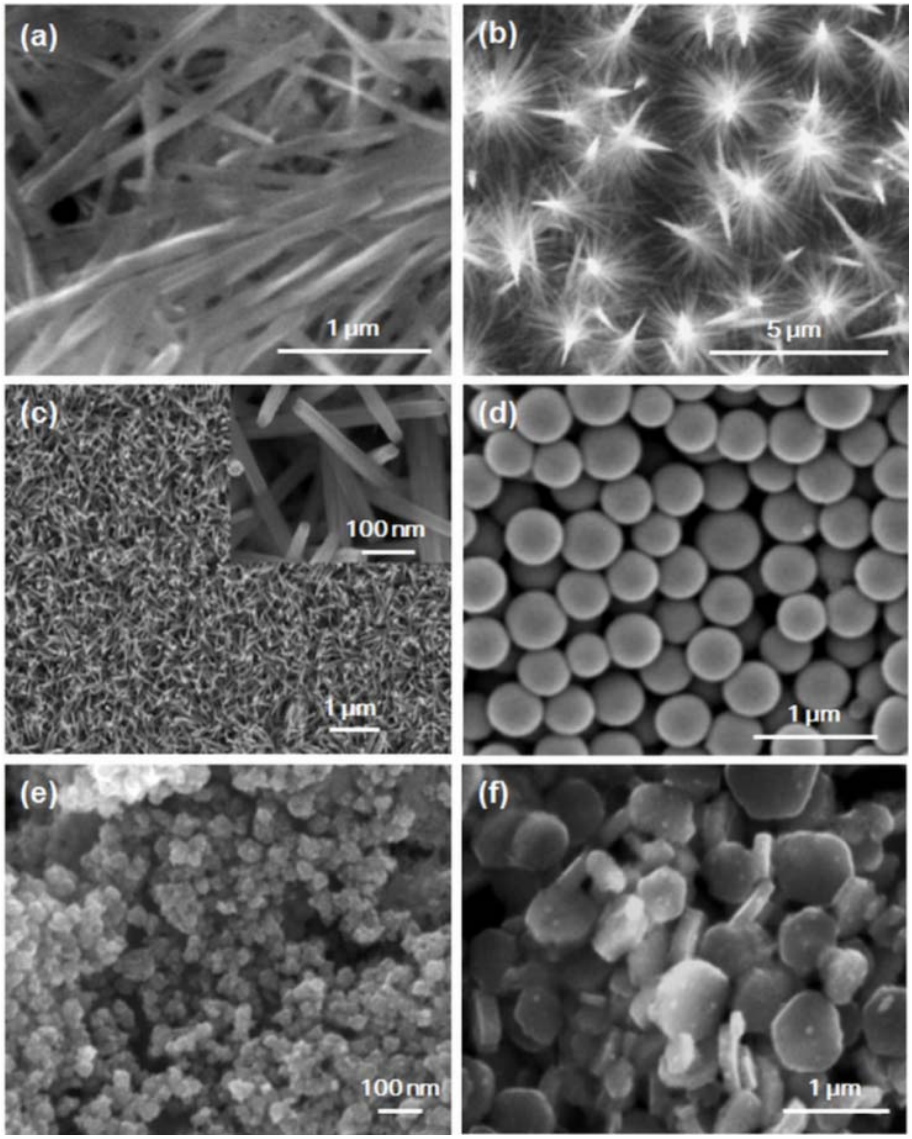

Figure 5: Scanning electron microscopy (SEM) images show the morphologies of the hydrothermally synthesized Nb_2O_5. (a) Nb_2O_5-nanosheets synthesized from NbO_2 precursor at 130 °C for 30 days, (b) Nb_2O_5-nanotrees synthesized from niobium foil dipped in HF acid solution and lithium hydroxide of pH=3.3-3.4 at 150-200 °C for 20-40 h, (c) Nb_2O_5-nanorods synthesized at 150 °C for 48 h in NH_4F aqueous solution of 0.02 M concentration, (d) Nb_2O_5-mesoporous spheres synthesized using niobium ethoxide mixed with DEG solvent and acetone at 180 °C for 12 h, (e) Nb_2O_5-nanoparticles synthesized in ammonium niobium oxalate using a mix of distilled water and hydrogen peroxide kept at 100 °C for 12 h and (f) Nb_2O_5-hexagonal nanoplatelets synthesized in a mix of $NbCl_5$ in ethanol at pH =2.1 kept at a temperature of 235 °C for 90 h. (a) Reprinted with permission from ref. 86. Copyright 2010, Elsevier, (b) Reprinted with permission from ref. 172. Copyright 2010, IOP Publishing Ltd., (c) Reprinted with permission from ref. 173. Copyright 2011, Elsevier, (d) Reprinted with permission from ref. 171.

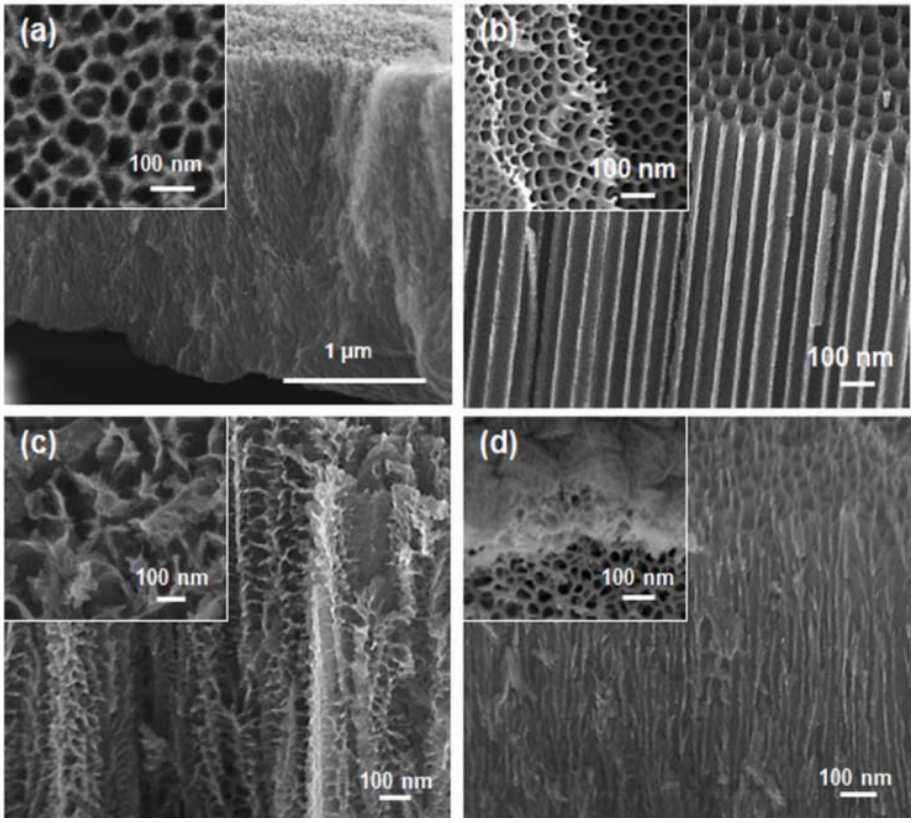

Figure 6: SEM images of: (a) Nb_2O_5 vein-like nanostructured networks and (b) Nb_2O_5 nanochannelled structure on foil; (c) nanoporous Nb_2O_5 and (d) nanochannelled Nb_2O_5 on FTO (the insets are top view images of the anodic films). (a) Reprinted with permission from ref. 23. Copyright 2012, American Chemical Society, (b) Reprinted with permission from ref. 22. Copyright 2014, Elsevier, (c,d) Reprinted with permission from ref. 110. Copyright 2013, The Royal Society of Chemistry.

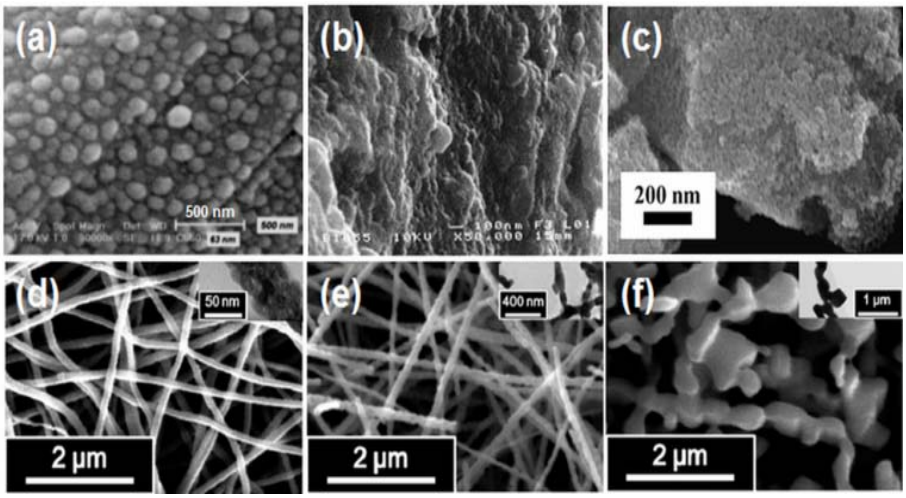

Figure 7: SEM images of annealed Nb_2O_5 prepared by (a, b, c) dip-coating sol-gel method and (d,e,f) electrospinning sol-gel method. (a) Reprinted with permission from ref. 125. Copyright 2012, Springer, (b) Reprinted with permission from ref. 121. Copyright 1999, Elsevier, (c) Reprinted with permission from ref. 124. Copyright 2012, Elsevier, (d,e,f) Reprinted with permission from ref. 27. Copyright 2010, American Chemical Society.

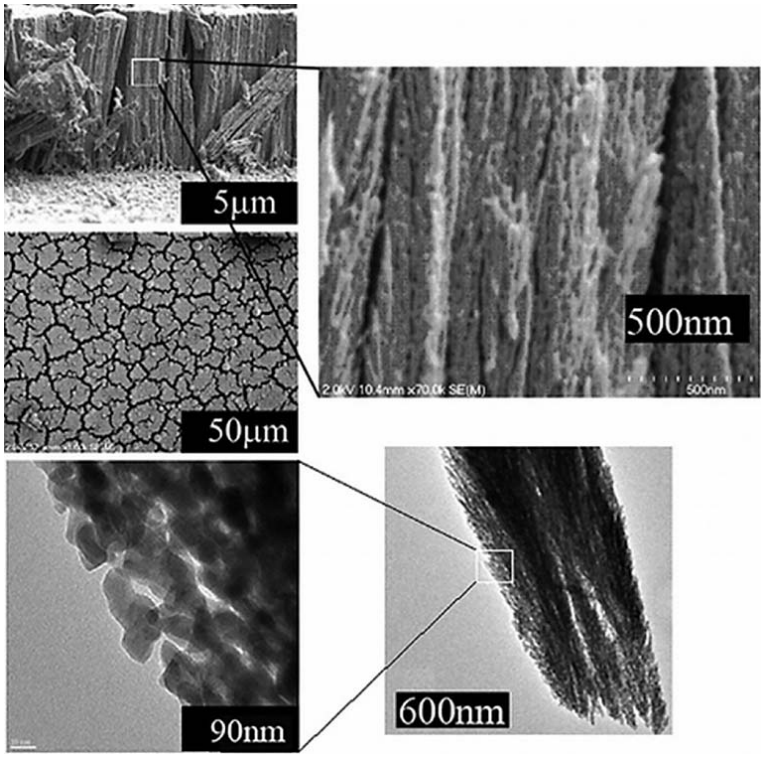

Figure 8: Top and cross-sectional views (SEM and TEM images) of Nb_2O_5 films deposited using PLD process. Reprinted with permission from ref. 20. Copyright 2011, American Chemical Society.

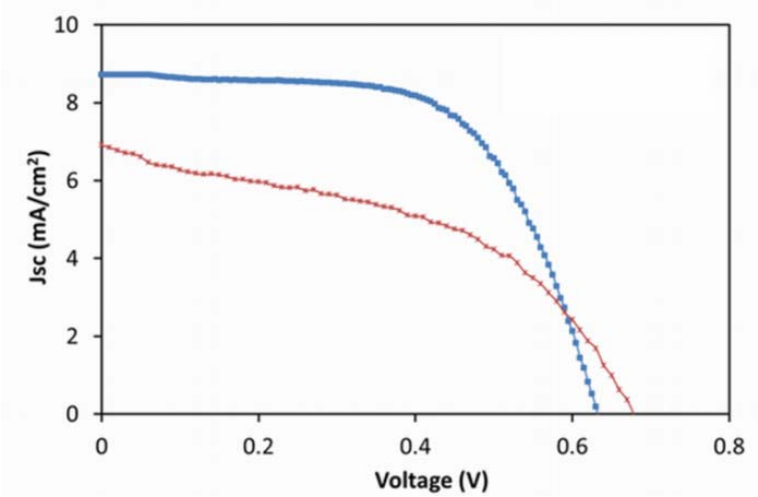

Figure 9: Current–voltage (*J–V*) characteristics of DSSCs fabricated using Nb_2O_5 without impurity defects (blue line) and Nb_2O_5 with impurity defects (red line) in the photoanodes. Reprinted with permission from ref. 110. Copyright 2013, Royal Society of Chemistry.

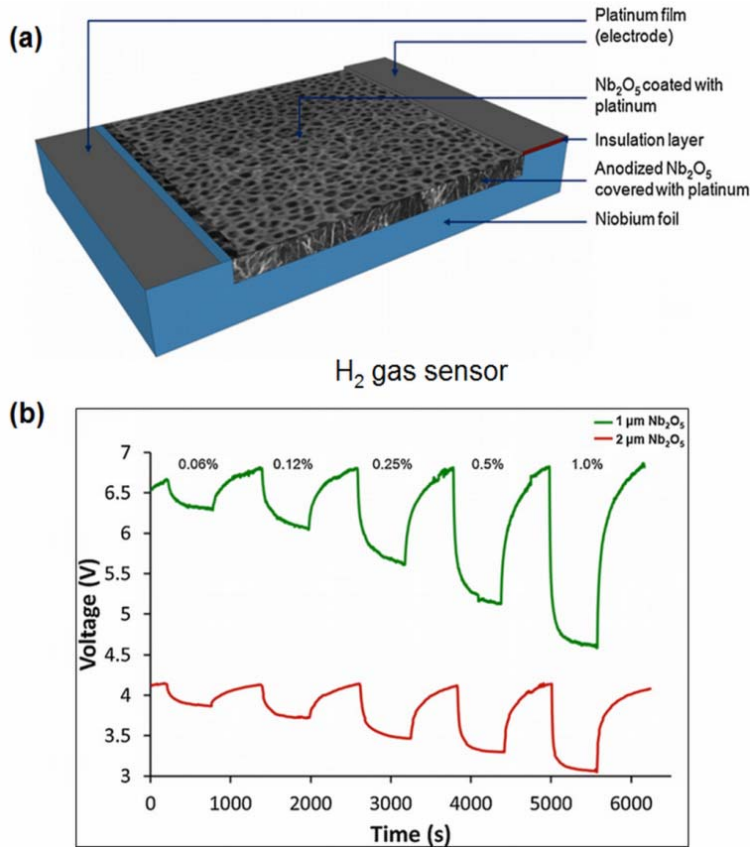

Figure 10: (a) The schematic of a Schottky based gas sensor made of nanoporous Nb_2O_5 coated with Pt and (b) dynamic response of such Nb_2O_5 gas sensors with 1 and 2 μm thick layers measured with different concentrations of H_2 gas at 100 °C at a constant bias current of 100 μA. Reprinted with permission from ref. 211. Copyright 2013, Elsevier.

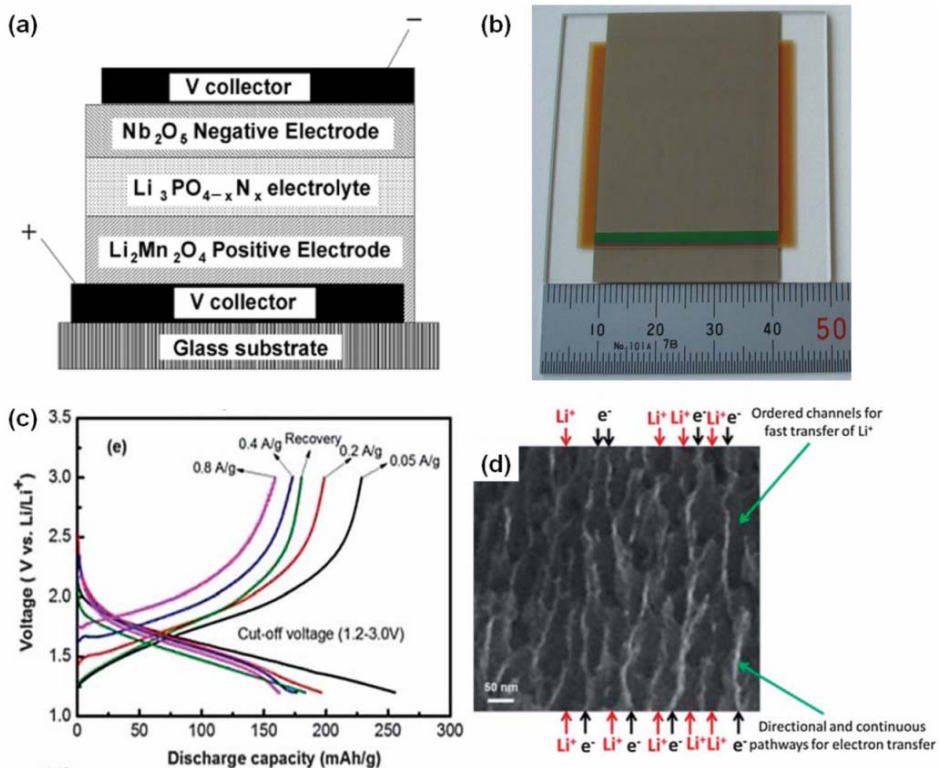

Figure 11: (a) A schematic diagram of a thin-filmed $Nb_2O_5/Li_2Mn_2O_4$ battery in a cross-section, and (b) a photograph of a thin-film battery with a 50 mm × 50 mm size in a plane view. (c) Electrochemical performance of the nanoporous Nb_2O_5 electrodes: corresponding galvanostatic discharge–charge voltage profiles for the 1st cycle at each rate. (d) The porous network of Nb_2O_5 with possible fast pathways for Li ions and electrons. (a,b) Reprinted with permission from ref. 238. Copyright 2007, Elsevier, (c,d) Reprinted with permission from ref. 103. Copyright 2013, The Royal Society of Chemistry.

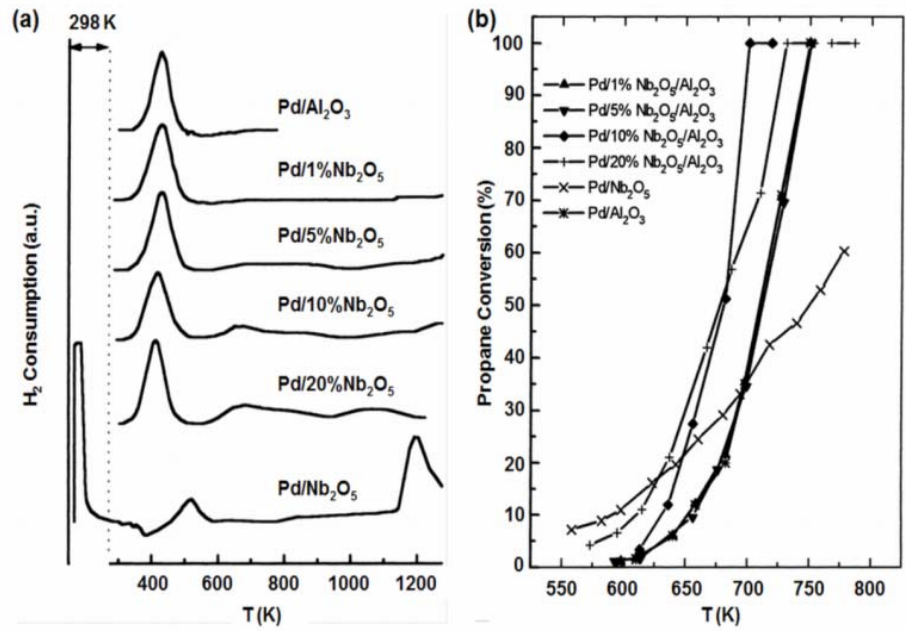

Figure 12: (a) Temperature-programmed reduction (TPR) profile of $Pd/Nb_2O_5/Al_2O_3$ catalysts. (b) Conversion of propane as a function of the reaction temperature for $Pd/Nb_2O_5/Al_2O_3$ catalysts at different ratios. Reprinted with permission from ref. 256. Copyright 2000, Elsevier.

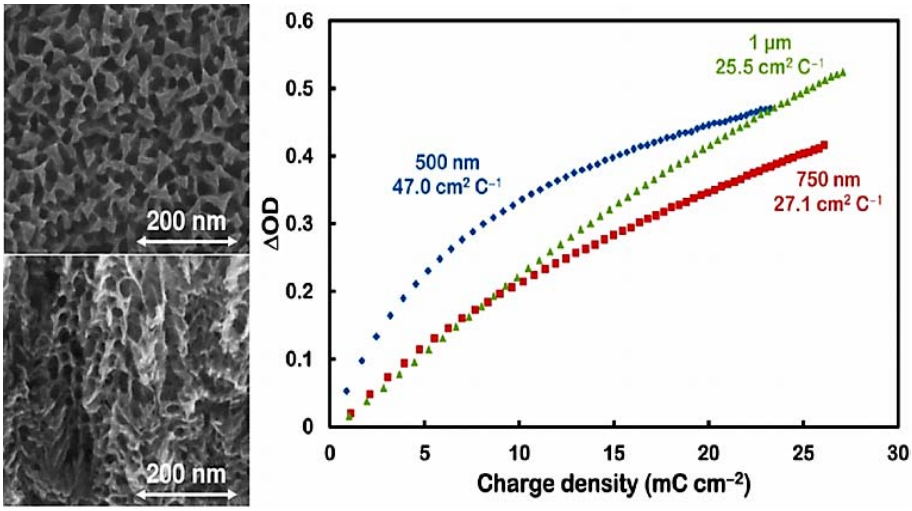

Figure 13: SEM images of anodized Nb_2O_5 films and the coloration efficiency of 500 nm, 750 nm, and 1 μm thick anodized Nb_2O_5 films under chronoamperometric (CA) at ±1.5 V applied potential for the optical wavelength of 550 nm. Reprinted with permission from ref. 69. Copyright 2014, American Chemical Society.